A COMPUTER METHOD FOR DESIGN AND ULTIMATE STRENGTH CAPACITY EVALUATION OF PRESTRESSED REINFORCED AND COMPOSITE STEEL-CONCRETE CROSS-SECTIONS

Cosmin G. CHIOREAN*

Technical University of Cluj-Napoca, Faculty of Civil Engineering, 15 C Daicoviciu Str., 400020, Cluj-Napoca, Romania

ABSTRACT

This paper presents a general method for the rapid design and ultimate strength capacity evaluation of arbitrary-shaped composite steel-concrete and prestressed reinforced cross-sections that are subjected to biaxial bending and axial force. The proposed iterative procedure adopts Newton-Raphson procedure and the arc-length constraint equation combined with the Green's theorem for transforming stress resultant and stiffness coefficients into line integrals, thus resulting in a high rate of convergence. The proposed approach has been found to be very stable for all cases examined herein even when the section is close to the state of pure compression or tension or when there are multiple solutions, and it is not sensitive to prestressing, to the initial or starting values, to how the origin of the reference loading axes is chosen, to the strain softening exhibited by concrete in compression and to the tension stiffening effect exhibited by the concrete in tension. A computer program was developed, aimed at obtaining the ultimate strength capacity and reinforcement required by prestressed reinforced and composite cross-sections subjected to combined biaxial bending and axial load. In order to illustrate the proposed method and its accuracy and efficiency, this program was used to study several representative examples, which have been studied previously by other researchers. The examples run and the comparisons made prove the effectiveness of the proposed method of analysis.

Keywords: Interaction diagrams; Rapid design; Composite cross-sections; Prestressed reinforced concrete; Ultimate strength analysis; Arc-length method; Fully yield surfaces; Biaxial bending.

1. INTRODUCTION

With the rapid advancement of computer technology, research works are currently in full swing to develop advanced nonlinear inelastic analysis methods of 3D frameworks, that involve accurate predictions of inelastic limit states up to or beyond structural collapse, and integrate them into the new and more rational advanced analysis and pushover design

* Tel./ Fax.:+40 264 594967

E-mail address: cosmin.chiorean@mecon.utcluj.ro (C.G. Chiorean)

procedures. One of the key issue in developing of such procedures represents the high accuracy and computational efficiency evaluation of elasto-plastic behaviour of cross-sections subjected to axial force and biaxial bending moments [1,2].

In recent years, some methods have been presented for the ultimate strength analysis and design of various concrete and composite steel-concrete sections. [3-18]. Among several existing techniques developed for ultimate strength capacity evaluation, two are the most common; the first consists of a direct generation of points of the failure surface by varying the position and inclination of the neutral axis (angle θ in Fig. 1) and imposing a strain distribution corresponding to a failure condition. This technique generates the failure surface through 3D curves, making the application of this technique rather cumbersome for practical applications. The second approach is based upon the solution of the non-linear equilibrium equations according to the classical Newton's scheme consisting of an iterative sequence of linear predictions and non-linear corrections to obtain either the strain distribution or the location and inclination of the neutral axis which determines the ultimate load, where one or two components of the section forces can remain constant. There exist three different methods to generate plane interaction curves for cross-sections under biaxial bending: (1) interaction curves for a given bending moment ratio *N-M-M,* [7], (2) load contours for a given axial load (*M-M*) [9] and (3) generate triplets of stress-resultants on the failure surface by extending an arbitrary oriented straight line [3, 6, 12, 13].

Numerical procedures that allow the design of steel reinforcements for sections subjected to biaxial bending and axial force have been proposed in several papers [5, 7, 9, 17]. Dundar and Sahin [5] presented a procedure based on the Newton-Raphson method for dimensioning of arbitrarily shaped reinforced concrete sections, subjected to combined biaxial bending and axial compression. In their analysis the distribution of concrete stress is assumed to be

rectangular according with Whitney's rectangular block. Rodrigues and Ochoa [7] extended this method for the more general cases when the concrete in compression is modelled using the explicit nonlinear stress-strain relationships. Chen *et.al.* [9] proposed an iterative quasi-Newton procedure based on the Regula-Falsi numerical scheme for the rapid sectional design of short concrete-encased composite columns of arbitrary cross-section subjected to biaxial bending. This algorithm is limited to fully confined concrete. More recently, Pallares *et.al.* [17], presents a new iterative algorithm to design the steel reinforcement of concrete sections subjected to axial forces and biaxial bending. This method is based on the ultimate strains proposed by Eurocode-2 for sections under uniaxial bending and is limited also to fully confined concrete. For all these algorithms, problems of convergence may arise especially when starting or initial values (i.e. the parameters that define the strain profile over the cross-section) are not properly selected, and they may become unstable near the state of pure compression or tension.

The present paper extends the previous study, carried out by the author [18] in the following two respects: (i) the procedure developed in [18] for construction of moment capacity contours and interaction diagrams is enhanced by inclusion of concrete tension stiffening effect and also to prestressed reinforced concrete sections and (ii) a new procedure based on Newton iterative method is proposed to design the required reinforcement for sections subjected to axial force and biaxial bending moments.

The proposed iterative approach adopts Newton-Raphson procedure and the arc-length constraint equation combined with the Green's theorem for transforming stress resultant and stiffness coefficients into line integrals, thus resulting in a high rate of convergence.

Concerning the ultimate strength capacity evaluation of cross-sections the proposed incremental-iterative method is advantageous with respect to the existing ones [7,9,16], in that the solution is obtained by solving just two coupled nonlinear equations and the convergence

stability is not affected to the initial/starting values of the basic variables (i.e. the ultimate curvatures about global axes ϕ_x and ϕ_y), involved in the iterative process. For all cases examined herein has been found that starting the iterative process with the initial curvatures ϕ_x=0 and ϕ_y=0 the convergence is achieved in a low number of iterations. Using the proposed method we have found that near the axial load capacity under pure compression, when the strain-softening of the concrete is taken into account, the solution is not unique which implies non-convexity of the failure surface in these situations. Therefore, the proposed approach based on arc-length constraint strategy is essential to assure the convergence of the entire process and to determine all possible solutions.

The method proposed herein, for design of cross-sections, consists of computing the required reinforcement area (A_{tot}) supposing that all structural parameters are specified and, under given external loads, the cross section reaches its failure either in tension or compression. The problem is formulated by means of three equilibrium equations for the section. The condition of ultimate limit state is enforced by a compatibility equation imposing the maximum strain on the section to be equal to the limit strain of the corresponding material. These nonlinear equations are manipulated so that one of them is uncoupled and the Newton iterative strategy is applied only to the remaining coupled equilibrium equations. The proposed approach is advantageous with respect to the existing ones [5, 7, 9, 17], in that the solution is obtained by solving just three coupled nonlinear equations [17] and the convergence stability is not sensitive to the initial/starting values of the basic variables [5, 7, 9] (i.e. the ultimate sectional curvatures ϕ_x and ϕ_y) involved in the iterative process. This method, as compared to other iterative methods used in the solution of nonlinear equations for design of cross-sections, is very stable, converging rapidly if the initial value of the required reinforcement area, A_{tot}, is properly selected. The stability and rapid convergence of the proposed approach is also due to the fact that the Jacobian's of the nonlinear system of

equations is explicitly computed whereas in the methods proposed by Dundar and Sahin [5] and Rodrigues and Ochoa [7], the partial derivatives, involved in determination of the Jacobian matrix, can be only approximately expressed in terms of finite differences.

2. MATHEMATICAL FORMULATION

2.1. Basic assumptions and constitutive material models

Consider the cross-section subjected to the action of the external bending moments about both global axes and axial force as shown in Figure 1. The cross-section may assume any shape with multiple polygonal or circular openings. It is assumed that plane section remains plane after deformation. This implies a perfect bond between the steel and concrete components of a composite concrete-steel cross section. Shear and torsional interaction effects are not accounted for in the concrete constitutive model. Thus the resultant strain distribution corresponding to the curvatures about global axes $\mathbf{\Phi}=\{\phi_x,\ \phi_y\}$ and the axial compressive strain ε_0 can be expressed at a generic point, in concrete matrix, fiber of structural steel or ordinary reinforced bars, of coordinates (x, y) in a linear form as:

$$\varepsilon = \varepsilon_0 + \phi_x y + \phi_y x \tag{1}$$

The strain in the prestressing bars is equal to the strain in the surrounding concrete, at the same level of the section, plus the initial strain imposed to the presetressed steel during its tensioning:

$$\varepsilon_{ps} = \varepsilon_c + \Delta\varepsilon_p \tag{2}$$

The relaxation of the prestressed steel can be accounted for by considering the time-dependent modulus of elasticity.

Behaviour of concrete in compression

Two stress-strain relationships are taken into account, in the present investigation, to model the compressive behaviour of concrete. The first constitutive relation [7] to model the concrete under compression is represented by a combination of a second-degree parabola (for ascending part) and a straight line (for descending part), Eq.(2), as depicted in Fig.2.a:

$$f_c = \begin{cases} f_c^{''}\left(2\dfrac{\varepsilon_c}{\varepsilon_{c0}} - \dfrac{\varepsilon_c^{\,2}}{\varepsilon_{c0}^2}\right), & \varepsilon_c \le \varepsilon_0 \\ f_c^{''}\left(1-\gamma\left(\dfrac{\varepsilon_c - \varepsilon_{c0}}{\varepsilon_{cu} - \varepsilon_{c0}}\right)\right), & \varepsilon_0 < \varepsilon_c \le \varepsilon_{cu} \end{cases} \tag{3}$$

where γ represents the degree of confinement in the concrete and allows for the modelling of strain-softening, creep and confinement in concrete by simply varying the crushing strain ε_{c0}, ultimate compressive strain ε_{cu} and γ respectively. The second constitutive relationship to model compressive behaviour of concrete is the stress-strain law prescribed by Eurocode 2 [14], as depicted in Fig.2.b:

$$f_c = f_c^{''}\frac{k\left(\dfrac{\varepsilon_c}{\varepsilon_{c0}}\right) - \left(\dfrac{\varepsilon_c}{\varepsilon_{c0}}\right)^2}{1+(k-2)\dfrac{\varepsilon_c}{\varepsilon_{c0}}}, \quad \varepsilon_c \le \varepsilon_{cu} \tag{4}$$

where

$$k = 1.1E_c\frac{\varepsilon_{c0}}{f_c^{''}} \tag{5}$$

and where $f_c^{''}$ represents the concrete cylindrical compressive strength, ε_{c0} the crushing strain, ε_{cu} the ultimate compressive strain and E_c denotes the modulus of elasticity of concrete in compression.

Behaviour of concrete in tension

Tension stiffening is an important phenomenon that should be included for an accurate analysis of sections under biaxial bending and axial load. Neglecting tension strength of concrete could lead to a loss in the smoothness of moment-curvature curves due to the sudden drop in stress from the cracking strength to zero at the onset cracking. In addition, tension stiffening results in a small change in peak strength, but this is usually negligible. The model to account for tension stiffening, developed by Vecchio & Collins [19] is taken into account in the present investigation. The model of concrete in tension can be given in the following analytical form (Fig. 3):

$$f_t = \begin{cases} E_t \varepsilon_c, \ \ \varepsilon_c \le \varepsilon_{cr} \\ \dfrac{\alpha_1 \alpha_2^2}{1+\sqrt{500\varepsilon_c}} f_{cr}, \varepsilon_c > \varepsilon_{cr} \end{cases} \tag{6}$$

where E_t denotes the modulus of elasticity of concrete in tension; f_{cr} represents the tensile strength of concrete; ε_{cr} is the concrete cracking strain; α_1 is a factor that takes into account the bounding characteristics of the reinforcement and α_2 represents a factor that takes into account the effects of load duration and cyclic loads. As illustrated in Figure 3 a slow rate of tension softening is assumed for the concrete in tension.

Behaviour of steel reinforcement

Multi-linear elastic-plastic stress-strain relationships, both in tension and in compression, is assumed for the structural steel and the conventional reinforcing bars. In this way the strain-hardening effect may be included in analysis. The analytical model can be given in the following form (Fig. 4):

$$f_s = \begin{cases} E_s \varepsilon, \ \ |\varepsilon| \le |\varepsilon_{sy1}| \\ \mathrm{sgn}(\varepsilon) f_{y1} + E_{sh1}\left(\varepsilon - \mathrm{sgn}(\varepsilon)\cdot \varepsilon_{sy1}\right), \varepsilon_{sy1} < |\varepsilon| \le \varepsilon_{sy2} \\ \mathrm{sgn}(\varepsilon) f_{y2} + E_{sh2}\left(\varepsilon - \mathrm{sgn}(\varepsilon)\cdot \varepsilon_{sy2}\right), \varepsilon_{sy2} < |\varepsilon| \le \varepsilon_{su} \end{cases} \tag{7}$$

where E_s is the Young modulus, f_{syi} denotes the yield stresses, ε_{syi} represents the yield strains, ε_{su} the ultimate steel strain and E_{shi} represents the slopes of the yielding branch.

Behaviour of prestressed steel

The constitutive relation to model prestressed steel bars is represented by multi-linear elastic-plastic stress-strain relationships, both in tension and compression, as already described in the case of ordinary reinforcing steel bars (Fig. 4):

$$f_{ps} = \begin{cases} E_{ps}\varepsilon_{ps}, \ \left|\varepsilon_{ps}\right| \le \left|\varepsilon_{psy1}\right| \\ \operatorname{sgn}(\varepsilon_{ps}) f_{psy1} + E_{psh1}\left(\varepsilon_{ps} - \operatorname{sgn}(\varepsilon_{ps}) \cdot \varepsilon_{psy1}\right), \varepsilon_{psy1} < \left|\varepsilon_{ps}\right| < \varepsilon_{psy2} \\ \operatorname{sgn}(\varepsilon_{ps}) f_{psy2} + E_{psh2}\left(\varepsilon_{ps} - \operatorname{sgn}(\varepsilon_{ps}) \cdot \varepsilon_{psy2}\right), \varepsilon_{psy2} < \left|\varepsilon_{ps}\right| < \varepsilon_{psu} \end{cases} \tag{8}$$

where E_{ps} is the Young modulus of prestressed steel, f_{psyi} denotes the yield stresses of prestressed steel, ε_{psyi} represents the yield strains of prestressed steel, ε_{psu} the ultimate prestressed steel strain and E_{pshi} represents the slopes of the yielding branch of presetressed steel.

2.2 Design procedure

An iterative procedure based on Newton method is proposed to design a cross-section subjected to axial force (N) and biaxial bending moments (M_x,, M_y). The method proposed herein consists of computing the required conventional reinforcement area (A_{tot}) supposing that all structural parameters are specified and, under given external loads, the cross section reach its failure either to maximum strains attained at the outer compressed point of the concrete section or to maximum strains attained in the most tensioned steel fibre.

Consider an irregular composite section as shown in Figure 1 subjected to axial force and biaxial bending moments. The global x, y -axes of the cross section could have their origin either in the elastic or plastic centroid of the cross-section. The conventional reinforcement

layout is given as percentage (α_i) of the total reinforcement steel area (A_{tot}) in each location. At ultimate strength capacity the equilibrium is satisfied when the external forces are equal to the internal ones and either in the most compressed or tensioned steel fibre the ultimate strain is attained. These conditions can be represented mathematically in terms of the following nonlinear system of equations as:

$$\begin{cases} \int_{A_{cs}} \sigma\left(\varepsilon\left(\varepsilon_0,\phi_x,\phi_y\right)\right)dA_{cs} + A_{tot}\sum_{i=1}^{N_{rs}} \sigma\left(\varepsilon_i\left(\varepsilon_0,\phi_x,\phi_y\right)\right)\alpha_i + \sum_{j=1}^{N_{ps}} \sigma\left(\varepsilon_j\left(\varepsilon_0,\phi_x,\phi_y\right)\right)A_{psj} - N = 0 \\ \int_{A_{cs}} \sigma\left(\varepsilon\left(\varepsilon_0,\phi_x,\phi_y\right)\right)y dA_{cs} + A_{tot}\sum_{i=1}^{N_{rs}} \sigma\left(\varepsilon_i\left(\varepsilon_0,\phi_x,\phi_y\right)\right)y_i\alpha_i + \sum_{j=1}^{N_{ps}} \sigma\left(\varepsilon_j\left(\varepsilon_0,\phi_x,\phi_y\right)\right)A_{psj}y_j - M_x = 0 \\ \int_{A_{cs}} \sigma\left(\varepsilon\left(\varepsilon_0,\phi_x,\phi_y\right)\right)x dA_{cs} + A_{tot}\sum_{i=1}^{N_{rs}} \sigma\left(\varepsilon_i\left(\varepsilon_0,\phi_x,\phi_y\right)\right)x_i\alpha_i + \sum_{j=1}^{N_{ps}} \sigma\left(\varepsilon_j\left(\varepsilon_0,\phi_x,\phi_y\right)\right)A_{psj}x_j - M_y = 0 \\ \varepsilon_0 + \phi_x y_c\left(\phi_x,\phi_y\right) + \phi_y x_c\left(\phi_x,\phi_y\right) - \varepsilon_u = 0 \end{cases} \tag{9}$$

in which A_{tot}, $\varepsilon_0, \phi_x, \phi_y$ represent the unknowns, the surface integral is extended over concrete and structural steel areas (A_{cs}), N_{rs} and N_{ps} represents the number of conventional steel reinforcement and prestressed bars respectively, and A_{psj} ($j=1,N_{ps}$) denotes the area of prestressed tendons. In the above equations the first three relations represent the basic equations of equilibrium for the axial load N and the biaxial bending moments $M_{x,}$, M_y respectively. The last equation represents the ultimate strength capacity condition, that is, in the most compressed or most tensioned point the ultimate strain is attained; in this equation $x_c\left(\phi_x,\phi_y\right)$and $y_c\left(\phi_x,\phi_y\right)$ represent the coordinates of the point in which this condition is imposed. The coordinates of the "constrained" point can be always determined for each inclination of the neutral axis defined by the parameters ϕ_x and ϕ_y, and ε_u represents the ultimate strain either in most compressed concrete point or in most tensioned steel fibre. The stresses in Equations (9) are calculated using the fiber strains and the constitutive relations.

For each inclination of the neutral axis defined by the parameters ϕ_x and ϕ_y the farthest point on the compression side (or the most tensioned reinforcement steel bar) is determined

(i.e. the point with co-ordinates x_c, y_c). We assume that at this point the failure condition is met:

$$\varepsilon_0 + \phi_x y_c + \phi_y x_c = \varepsilon_u \tag{10}$$

Hence, the axial strain ε_0 can be expressed as:

$$\varepsilon_0 = \varepsilon_u - \left(\phi_x y_c + \phi_y x_c\right) \tag{11}$$

Taking into account Eq.(1), the resulting strain distribution corresponding to the curvatures ϕ_x and ϕ_y can be expressed in linear form as:

$$\varepsilon\left(\phi_x, \phi_y\right) = \varepsilon_u + \phi_x\left(y - y_c\right) + \phi_y\left(x - x_c\right) \tag{12}$$

In this way, substituting the strain distribution given by the Eq.(12) in the basic equations of equilibrium, the unknown ε_0 together with the failure constraint equation can be eliminated from the nonlinear system (9). Thus, the nonlinear system of equations (9) is reduced to an only three basic equations of equilibrium as:

$$\begin{cases} f_1\left(\phi_x, \phi_y, A_{tot}\right) \equiv \int_{A_{cs}} \sigma\left(\varepsilon\left(\phi_x, \phi_y\right)\right) dA_{cs} + A_{tot} \sum_{i=1}^{N_{rs}} \sigma\left(\varepsilon_i\left(\phi_x, \phi_y\right)\right) \alpha_i + \sum_{j=1}^{N_{ps}} \sigma\left(\varepsilon_j\left(\phi_x, \phi_y\right)\right) A_{psj} - N = 0 \\ f_2\left(\phi_x, \phi_y, A_{tot}\right) \equiv \int_{A_{cs}} \sigma\left(\varepsilon\left(\phi_x, \phi_y\right)\right) y dA_{cs} + A_{tot} \sum_{i=1}^{N_{rs}} \sigma\left(\varepsilon_i\left(\phi_x, \phi_y\right)\right) y_i \alpha_i + \sum_{j=1}^{N_{ps}} \sigma\left(\varepsilon_j\left(\phi_x, \phi_y\right)\right) A_{psj} y_j - M_x = 0 \\ f_3\left(\phi_x, \phi_y, A_{tot}\right) \equiv \int_{A_{cs}} \sigma\left(\varepsilon\left(\phi_x, \phi_y\right)\right) x dA_{cs} + A_{tot} \sum_{i=1}^{N_{rs}} \sigma\left(\varepsilon_i\left(\phi_x, \phi_y\right)\right) x_i \alpha_i + \sum_{j=1}^{N_{ps}} \sigma\left(\varepsilon_j\left(\phi_x, \phi_y\right)\right) A_{psj} x_j - M_y = 0 \end{cases} \tag{13}$$

in which the unknowns, total reinforcement steel area A_{tot}, and the ultimate sectional curvatures ϕ_x and ϕ_y, can be obtained iteratively following the Newton method. In this respect, the system (13) can be rewritten in terms of non-linear system of equations in the following general form:

$$\mathbf{F}\left(\mathbf{X}\right) = \mathbf{f}^{\text{int}} - \mathbf{f}^{ext} = \mathbf{0} \tag{14}$$

where the external biaxial loading vector is:

$$\mathbf{f}^{ext} = \begin{bmatrix} N & M_x & M_y \end{bmatrix}^T \tag{15}$$

and the internal forces vector, computed as function of the curvatures and total reinforcement steel area A_{tot}, $\mathbf{X} = \begin{bmatrix} \phi_x & \phi_y & A_{tot} \end{bmatrix}^T$ is:

$$\mathbf{f}^{int} = \begin{bmatrix} N^{\text{int}} = \int_{A_{cs}} \sigma\left(\varepsilon\left(\phi_x, \phi_y\right)\right) dA_{cs} + A_{tot} \sum_{i=1}^{N_{rs}} \sigma\left(\varepsilon_i\left(\phi_x, \phi_y\right)\right)\alpha_i + \sum_{j=1}^{N_{ps}} \sigma\left(\varepsilon_j\left(\phi_x, \phi_y\right)\right) A_{psj} \\ M_x^{int} = \int_{A_{cs}} \sigma\left(\varepsilon\left(\phi_x, \phi_y\right)\right) y dA_{cs} + A_{tot} \sum_{i=1}^{N_{rs}} \sigma\left(\varepsilon_i\left(\phi_x, \phi_y\right)\right) y_i \alpha_i + \sum_{j=1}^{N_{ps}} \sigma\left(\varepsilon_j\left(\phi_x, \phi_y\right)\right) A_{psj} y_j \\ M_y^{int} = \int_{A_{cs}} \sigma\left(\varepsilon\left(\phi_x, \phi_y\right)\right) x dA_{cs} + A_{tot} \sum_{i=1}^{N_{rs}} \sigma\left(\varepsilon_i\left(\phi_x, \phi_y\right)\right) x_i \alpha_i + \sum_{j=1}^{N_{ps}} \sigma\left(\varepsilon_j\left(\phi_x, \phi_y\right)\right) A_{psj} x_j \end{bmatrix} \tag{16}$$

According to the Newton iterative method, the iterative changes of unknowns vector **X** can be written as:

$$\mathbf{X}^{k+1} = \mathbf{X}^k - \mathbf{F}' \left(\mathbf{X}^k\right)^{-1} \mathbf{F}\left(\mathbf{X}^k\right), k \geq 0 \tag{17}$$

where **F'** represents the Jacobian of the nonlinear system (13) and can be expressed as:

$$\mathbf{F}' = \left(\frac{\partial \mathbf{F}}{\partial \mathbf{X}}\right) = \begin{bmatrix} \frac{\partial N^{\text{int}}}{\partial \phi_x} & \frac{\partial N^{\text{int}}}{\partial \phi_y} & \frac{\partial N^{\text{int}}}{\partial A_{tot}} \\ \frac{\partial M_x^{\text{int}}}{\partial \phi_x} & \frac{\partial M_x^{\text{int}}}{\partial \phi_y} & \frac{\partial M_x^{\text{int}}}{\partial A_{tot}} \\ \frac{\partial M_y^{\text{int}}}{\partial \phi_x} & \frac{\partial M_y^{\text{int}}}{\partial \phi_y} & \frac{\partial M_y^{\text{int}}}{\partial A_{tot}} \end{bmatrix} \tag{18}$$

Explicitly the expressions of the Jacobian's coefficients are:

$$\begin{aligned}
\frac{\partial N^{\text{int}}}{\partial \phi_x} &= \int_{A_{cs}} E_t (y - y_c) dA_{cs} + A_{tot} \sum_{i=1}^{N_{rs}} E_{ti} (y_i - y_c) \alpha_i + \sum_{j=1}^{N_{ps}} E_{tj} (y_i - y_c) A_{psj} \\
\frac{\partial N^{\text{int}}}{\partial \phi_y} &= \int_{A_{cs}} E_t (x - x_c) dA_{cs} + A_{tot} \sum_{i=1}^{N_{rs}} E_{ti} (x_i - x_c) \alpha_i + \sum_{j=1}^{N_{ps}} E_{tj} (x_j - y_c) A_{psj} \\
\frac{\partial N^{\text{int}}}{\partial A_{tot}} &= \sum_{i=1}^{N_{rs}} \sigma(\varepsilon_i) \alpha_i \\
\frac{\partial M_x^{\text{int}}}{\partial \phi_x} &= \int_{A_{cs}} E_t y (y - y_c) dA_{cs} + A_{tot} \sum_{i=1}^{N_{rs}} E_{ti} y_i (y_i - y_c) \alpha_i + \sum_{j=1}^{N_{ps}} E_{tj} y_j (y_j - y_c) A_{psj} \\
\frac{\partial M_x^{\text{int}}}{\partial \phi_y} &= \int_{A_{cs}} E_t y (x - x_c) dA_{cs} + A_{tot} \sum_{i=1}^{N_{rs}} E_{ti} y_i (x_i - x_c) \alpha_i + \sum_{j=1}^{N_{ps}} E_{tj} y_j (x_j - x_c) A_{psj} \\
\frac{\partial M_x^{\text{int}}}{\partial A_{tot}} &= \sum_{i=1}^{N_{rs}} \sigma(\varepsilon_i) y_i \alpha_i \\
\frac{\partial M_y^{\text{int}}}{\partial \phi_x} &= \int_{A_{cs}} E_t x (y - y_c) dA_{cs} + A_{tot} \sum_{i=1}^{N_{rs}} E_{ti} x_i (y_i - y_c) \alpha_i + \sum_{j=1}^{N_{ps}} E_{tj} x_j (y_j - y_c) A_{psj} \\
\frac{\partial M_y^{\text{int}}}{\partial \phi_y} &= \int_{A_{cs}} E_t x (x - x_c) dA_{cs} + A_{tot} \sum_{i=1}^{N_{rs}} E_{ti} x_i (x_i - x_c) \alpha_i + \sum_{j=1}^{N_{ps}} E_{tj} x_j (x_j - x_c) A_{psj} \\
\frac{\partial M_y^{\text{int}}}{\partial A_{tot}} &= \sum_{i=1}^{N_{rs}} \sigma(\varepsilon_i) x_i \alpha_i
\end{aligned} \tag{19}$$

These coefficients are expressed in terms of the tangent modulus of elasticity E_t, total reinforcement steel area A_{tot} and the coordinates x_c, y_c of the "constrained" point. As already mentioned, during the iterative process, for each inclination of the neutral axis defined by the current curvatures, ϕ_x and ϕ_y, the coordinates of the constrained point can be always determined and consequently the stiffness matrix coefficients can be evaluated. The iterative procedure starts with curvatures $\phi_x=0$, $\phi_y=0$. At the very first iteration, starting with the initial curvatures $\phi_x=0$ and $\phi_y=0$ the Jacobian **F'** could become singular, because in this case the strain profile over the cross-section is uniform with maximum ultimate strain in compression or tension, which implies zero tangent modulus of elasticity. In this case one can simply start the iteration process with the secant modulus of elasticity in the evaluation of the tangent stiffness coefficients of the cross-section. For the next iterations an adaptive-descent algorithm [20] is applied in order to avoid the convergence difficulties related to negative-definition of the Jacobian matrix that can occur during the iterative process. Adaptive descent is a technique which switches to a secant matrix if convergence difficulties are encountered, and switches back to the full tangent as the solution convergences, resulting in the desired rapid convergence rate. The third variable of the starting triplet, initial total reinforcement steel area A_{tot}, can be chosen as a percentage of the gross concrete cross-sectional area. The initial approximation for A_{tot} is chosen by the user of the computer program, and represents the only parameter that controls the stability of convergence process. If the initial value of A_{tot} is taken to be $0.005A_g$ (i.e. A_g is gross cross-sectional area) it is observed that the iterative process described above has converged for many different problems in six to seven iterations. However, it was found that, sometimes, the iterative algorithm may converge to a negative value for the reinforcement steel area. In this case, using a trial and error process, the user has to restart the process with different initial values for total reinforcement steel area and searched for, in this way, the positive solution of the problem.

The convergence criterion is expressed as a ratio of the norm of the out-of-balance force vector to the norm of the applied load. So the solution is assumed to have converged if:

$$\frac{\sqrt{\mathbf{F}^T\mathbf{F}}}{\sqrt{\mathbf{f}^{extT}\mathbf{f}^{ext}}} \leq TOL \tag{20}$$

where *TOL* is the specified computational tolerance, usually taken as 1*E*-4. As it was stated previously, the failure of the cross section can be controlled either by the most compressed concrete point or the most tensioned steel reinforcement bar. For a compression axial force, the iterative process is started with control in compression, whereas for a tension axial force the design of the cross-section is conducted starting the iterative process imposing the failure of the cross section in tension. During the iterative process these controlled points are automatically interchanged. For instance, assuming that the current iterations are conducted with the most compressed point (Fig. 5) the strains profiles are defined by the same ultimate compressive strain and by different strains at the level of the most tensioned point. After the strains in the most tensioned point equal or exceed the tensile steel strain at failure, the control point becomes the most tensioned point, and the process continues similarly, but with the coordinates of this point and associated ultimate steel strain. Figure 5 presents different types of strain profiles during this process, defined by the either ultimate compressive strain (1,2,...) or by the ultimate steel strain (1',2',...). Figure 6 shows a simplified flowchart of this analysis algorithm.

2.3 Determination of the interaction diagrams and moment capacity contours

2.3.1 Problem definition and solution strategy

The proposed model is identical to that recently presented by the author in [18] except that the effects of tension stiffening and prestressing of steel bars are included. This model will be briefly described herein for easy reference and convenience.

The cross-section subjected to bi-axial bending moments and axial force, reaches its failure limit state when the strain in the extreme compression fiber of the concrete, or in the most tensioned reinforcement steel fiber, attains the ultimate value. Consequently, at ultimate strength capacity the equilibrium is satisfied when the external forces are equal to the internal ones and in the most compressed or tensioned point the ultimate strain is attained. These conditions can be represented mathematically in terms of the following nonlinear system of equations as:

$$\begin{cases} \int_{A_{cs}} \sigma\left(\varepsilon\left(\varepsilon_0,\phi_x,\phi_y\right)\right)dA_{cs} + \sum_{i=1}^{N_{rs}} \sigma\left(\varepsilon_i\left(\varepsilon_0,\phi_x,\phi_y\right)\right)A_{rsi} + \sum_{j=1}^{N_{ps}} \sigma\left(\varepsilon_j\left(\varepsilon_0,\phi_x,\phi_y\right)\right)A_{psj} - N = 0 \\ \int_{A_{cs}} \sigma\left(\varepsilon\left(\varepsilon_0,\phi_x,\phi_y\right)\right)y\,dA_{cs} + \sum_{i=1}^{N_{rs}} \sigma\left(\varepsilon_i\left(\varepsilon_0,\phi_x,\phi_y\right)\right)y_i A_{rsi} + \sum_{j=1}^{N_{ps}} \sigma\left(\varepsilon_j\left(\varepsilon_0,\phi_x,\phi_y\right)\right)A_{psj} y_j - M_x = 0 \\ \int_{A_{cs}} \sigma\left(\varepsilon\left(\varepsilon_0,\phi_x,\phi_y\right)\right)x\,dA_{cs} + \sum_{i=1}^{N_{rs}} \sigma\left(\varepsilon_i\left(\varepsilon_0,\phi_x,\phi_y\right)\right)x_i A_{rsi} + \sum_{j=1}^{N_{ps}} \sigma\left(\varepsilon_j\left(\varepsilon_0,\phi_x,\phi_y\right)\right)A_{psj} x_j - M_y = 0 \\ \varepsilon_0 + \phi_x y_c\left(\phi_x,\phi_y\right) + \phi_y x_c\left(\phi_x,\phi_y\right) - \varepsilon_u = 0 \end{cases} \quad (21)$$

in which N, M_x, M_y, $\varepsilon_0, \phi_x, \phi_y$ represent the unknowns, the surface integral is extended over concrete and structural steel areas (A_{cs}), N_{rs} and N_{ps} represents the number of conventional steel reinforcement and prestressed bars respectively, A_{rsi} ($i=1,N_{rs}$) and A_{psj} ($j=1,N_{ps}$) denotes the area of conventional steel and prestressed tendons respectively. In Eqs. (21) the first three relations represent the basic equations of equilibrium for the axial load N and the biaxial bending moments M_x,, M_y respectively, given in terms of the stress resultants. The last equation represents the ultimate strength capacity condition; in this equation $x_c(\phi_x,\phi_y)$ and $y_c(\phi_x,\phi_y)$ represent the coordinates of the point in which this condition is imposed. The coordinates of the "constrained" point can be always determined for each inclination of the neutral axis defined by the parameters ϕ_x and ϕ_y, and ε_u represents the ultimate strain either in most compressed concrete point or in most tensioned reinforcement steel fibre. Under the above assumptions, the problem of the ultimate strength analysis of composite (concrete-steel) cross-sections can be formulated as [18]:

Given a strain distribution corresponding to a failure condition, find the ultimate resistances N, M_x, M_y so as to fulfill the basic equations of equilibrium and one of the following linear constraints:

$$\begin{cases} L_1(N, M_x, M_y) \equiv M_x - M_{x0} = 0 \\ L_2(N, M_x, M_y) \equiv M_y - M_{y0} = 0 \end{cases} \tag{22}$$

$$\begin{cases} L_1(N, M_x, M_y) \equiv N - N_0 = 0 \\ L_2(N, M_x, M_y) \equiv M_x - M_{x0} = 0 \end{cases} \tag{23}$$

where N_0, M_{x0}, M_{y0} represent the given axial force and bending moments, respectively.

The general solution procedure is based on the solution of the nonlinear system (21) for one of two linear constraints defined by the Eqs. (22) and (23). Corresponding to each linear constraints we can define a point on the failure surface as: (I) when the constraints (22) are injected in the nonlinear system (21), a point on the failure surface is defined computing the axial resistance N associated with a failure criterion and for a fixed value of bending moments (M_x, M_y); (II) when constraints (23) are used, the point is associated with a fixed axial load (N) and a given bending moment M_x about x axis. This is then used as the basis for one of two analysis options: (1) a plot of the vertical sections of the failure surface that are typically called interaction diagrams, (2) a plot of the horizontal sections of the failure surface that are typically called moment capacity contours or loading contours. All these situations are graphically illustrated in Figure 7.

An incremental-iterative procedure based on arc-length constraint equation is proposed in order to determine the biaxial strength of an arbitrary composite steel-concrete and prestressed reinforced cross sections according to the already described situations. Consider an irregular composite section as shown in Figure 1. The failure diagrams correspond either to maximum strains attained at the outer compressed point of the concrete section (i.e. ε_u equal to the compressive strain at failure) or to maximum strains attained in the most tensioned reinforcement steel fibre (i.e. ε_u equal to the tensile steel strain at failure). For each inclination

of the neutral axis defined by the parameters ϕ_x and ϕ_y the farthest point on the compression side (or the most tensioned steel bar position) is determined (i.e. the point with co-ordinates x_c, y_c). Assuming that the failure condition is achieved in this point, the resulting strain distribution corresponding to the curvatures ϕ_x and ϕ_y can be expressed in linear form as in Eq.(12). Then, substituting the strain distribution given by the Eq. (12) in the basic equations of equilibrium, the unknown ε_0 together with the failure constraint equation can be eliminated from the nonlinear system (21). Thus, the nonlinear system of equations (21) is reduced to an only three basic equations of equilibrium and together with one linear constraint (Eq. 22 or Eq. 23), form a determined nonlinear system of equations, and the solutions can be obtained iteratively following an approach outlined in the next sections. It is important to note that the curvatures ϕ_x and ϕ_y, solutions of the above system of equations, are associated with a failure criterion and represent the ultimate sectional curvatures.

2.3.2 Interaction diagrams for given bending moments

In this case introducing the constraints (22) in the system (21), parametrizing the bending moments by a single variable λ (i.e. the load parameter) and regarding the ultimate curvatures ϕ_x and ϕ_y as independent variables in the axial force equation, the interaction diagram can be determined by solving the following two coupled equations:

$$\begin{cases} \int_{A_{cs}} \sigma\left(\varepsilon\left(\phi_x,\phi_y\right)\right) y dA_{cs} + \sum_{i=1}^{N_{rs}} \sigma\left(\varepsilon_i\left(\phi_x,\phi_y\right)\right) y_i A_{rsi} + \sum_{j=1}^{N_{ps}} \sigma\left(\varepsilon_j\left(\phi_x,\phi_y\right)\right) y_j A_{psj} - \lambda M_{x0} = 0 \\ \int_{A_{cs}} \sigma\left(\varepsilon\left(\phi_x,\phi_y\right)\right) x dA_{cs} + \sum_{i=1}^{N_{rs}} \sigma\left(\varepsilon_i\left(\phi_x,\phi_y\right)\right) x_i A_{rsi} + \sum_{j=1}^{N_{ps}} \sigma\left(\varepsilon_j\left(\phi_x,\phi_y\right)\right) x_j A_{psj} - \lambda M_{y0} = 0 \end{cases} \tag{24}$$

where the curvatures ϕ_x and ϕ_y and the load amplifier factor λ represent the unknowns and then the ultimate axial force, associated at a load amplifier factor λ (which define the intensity of the bending moments) can be directly evaluated as:

$$N = \int_{A_{cs}} \sigma\left(\varepsilon\left(\phi_x, \phi_y\right)\right) dA_{cs} + \sum_{i=1}^{N_{rs}} \sigma\left(\varepsilon_i\left(\phi_x, \phi_y\right)\right) A_{rsi} + \sum_{j=1}^{N_{ps}} \sigma\left(\varepsilon_j\left(\phi_x, \phi_y\right)\right) A_{psj} \tag{25}$$

In this way, for given bending moments we can obtain directly the axial force resistance N and a point on the failure surface associated with known bending moments. An incremental-iterative procedure based on arc-length constraint equation can be applied in order to solve the system (24). In this approach, the equations are solved in a series of steps or increments, usually starting from the unloaded state ($\lambda = 0$), and the solution of Eq. (24), referred to as equilibrium path, is obtained by solving directly the equilibrium equations together with an auxiliary constraint equation imposed for the load amplifier load factor. The system (24) can be rewritten in terms of non-linear system of equations in the following general form:

$$\mathbf{F}(\lambda, \mathbf{\Phi}) = \mathbf{f}^{\text{int}} - \lambda \mathbf{f}^{ext} = \mathbf{0} \tag{26}$$

where $\mathbf{f}^{ext} = \left[M_{x0} \quad M_{y0}\right]^T$ is the reference load vector (reference bending moments),

$$\mathbf{f}^{int} = \begin{bmatrix} M_x^{\text{int}} = \int_{A_{cs}} \sigma\left(\varepsilon\left(\phi_x, \phi_y\right)\right) y dA_{cs} + \sum_{i=1}^{N_{rs}} \sigma\left(\varepsilon_i\left(\phi_x, \phi_y\right)\right) y_i A_{rsi} + \sum_{j=1}^{N_{ps}} \sigma\left(\varepsilon_j\left(\phi_x, \phi_y\right)\right) y_j A_{psj} \\ M_y^{\text{int}} = \int_{A_{cs}} \sigma\left(\varepsilon\left(\phi_x, \phi_y\right)\right) x dA_{cs} + \sum_{i=1}^{N_{rs}} \sigma\left(\varepsilon_i\left(\phi_x, \phi_y\right)\right) x_i A_{rsi} + \sum_{j=1}^{N_{ps}} \sigma\left(\varepsilon_j\left(\phi_x, \phi_y\right)\right) x_j A_{psj} \end{bmatrix} \tag{27}$$

is the internal bending moments vector, computed as function of the curvatures $\mathbf{\Phi} = \left[\phi_x \quad \phi_y\right]^T$.

Applying an indirect solution scheme [21] for solving Eq.(26), the load increment is considered governed by the following constraint equation having the general form:

$$\Delta\mathbf{\Phi}^T \Delta\mathbf{\Phi} + \Delta\lambda^2 \Psi^2 \mathbf{f}^{extT} \mathbf{f}^{ext} - \Delta l^2 = 0 \tag{28}$$

where $\Delta\mathbf{\Phi}$ is the vector of curvatures, $\Delta\lambda$ is the incremental load-factor, Δl is the specified arc length for the current increment and Ψ is the scaling parameter for loading and curvature terms. According to the indirect arc-length technique, the iterative changes of curvature vector $\delta\mathbf{\Phi}$ for the new unknown load level $\Delta\lambda_{k+1} = \Delta\lambda_k + \delta\lambda$, is written as:

$$\delta\mathbf{\Phi} = -\mathbf{K}_T{}^{-1}\mathbf{F} + \delta\lambda\mathbf{K}_T{}^{-1}\mathbf{f}^{ext} = \delta\mathbf{F} + \delta\lambda\delta\mathbf{\Phi}_T \tag{29}$$

where $\mathbf{F}$ represents the out-of-balance force vector (Eq. 26) and $\mathbf{K}_T$ represents the tangent stiffness matrix of the cross-section:

$$\mathbf{K}_T = \left(\frac{\partial\mathbf{F}}{\partial\mathbf{\Phi}}\right) = \begin{bmatrix} \dfrac{\partial M_x{}^{int}}{\partial\phi_x} & \dfrac{\partial M_x{}^{int}}{\partial\phi_y} \\ \dfrac{\partial M_y{}^{int}}{\partial\phi_x} & \dfrac{\partial M_y{}^{int}}{\partial\phi_x} \end{bmatrix} \tag{30}$$

in which the partial derivatives are expressed with respect to the strains and stresses evaluated at current iteration k. Assuming the strain distribution given by the Eq.(12), the coefficients of the stiffness matrix can be symbolically evaluated as:

$$\begin{aligned}
k_{11} &= \frac{\partial M_x{}^{int}}{\partial\phi_x} = \int_{A_{cs}} E_T y(y-y_c)dA_{cs} + \sum_{i=1}^{N_{rs}} E_{ti} y_i (y_i - y_c) A_{rsi} + \sum_{j=1}^{N_{ps}} E_{tj} y_j (y_j - y_c) A_{psj} \\
k_{12} &= \frac{\partial M_x{}^{int}}{\partial\phi_y} = \int_{A_{cs}} E_T y(x-x_c)dA_{cs} + \sum_{i=1}^{N_{rs}} E_{ti} y_i (x_i - x_c) A_{rsi} + \sum_{j=1}^{N_{ps}} E_{tj} y_j (x_j - x_c) A_{psj} \\
k_{21} &= \frac{\partial M_y{}^{int}}{\partial\phi_x} = \int_{A_{cs}} E_T x(y-y_c)dA_{cs} + \sum_{i=1}^{N_{rs}} E_{ti} x_i (y_i - y_c) A_{rsi} + \sum_{j=1}^{N_{ps}} E_{tj} x_j (y_j - y_c) A_{psj} \\
k_{22} &= \frac{\partial M_y{}^{int}}{\partial\phi_y} = \int_{A_{cs}} E_T x(x-x_c)dA_{cs} + \sum_{i=1}^{N_{rs}} E_{ti} x_i (x_i - x_c) A_{rsi} + \sum_{j=1}^{N_{ps}} E_{tj} x_j (x_j - x_c) A_{psj}
\end{aligned} \tag{31}$$

where the coefficients k_{ij} are expressed in terms of the tangent modulus of elasticity E_t and the coordinates x_c, y_c of the "constrained" point. Thus the incremental curvatures for the next iteration can be written as:

$$\Delta\mathbf{\Phi}_{k+1} = \Delta\mathbf{\Phi}_k + \delta\mathbf{\Phi} \tag{32}$$

This procedure is iterated until convergence with respect to a suitable norm is attained. Assuming that a point (${}^{\tau}\mathbf{\Phi}$, ${}^{\tau}\lambda$) of the equilibrium path has been reached, the next point (${}^{\tau+\Delta\tau}\mathbf{\Phi}$, ${}^{\tau+\Delta\tau}\lambda$) of the equilibrium path is then computed updating the loading factor and curvatures as:

$$\begin{aligned}
{}^{\tau+\Delta\tau}\lambda &= {}^{\tau}\lambda + \Delta\lambda_{k+1} \\
{}^{\tau+\Delta\tau}\mathbf{\Phi} &= {}^{\tau}\mathbf{\Phi} + \Delta\mathbf{\Phi}_{k+1}
\end{aligned} \tag{33}$$

In this way, with curvatures and loading factor known, the axial force resistance N is computed on the basis of the resultant strain distribution corresponding to the curvatures ϕ_x and ϕ_y through equation (25), and the ultimate bending moments, M_x and M_y, are obtained scaling the reference external moments M_{x0} and M_{y0} through current loading factor λ given by Equation (33). Adopting an automatic step length adaptation scheme for the loading factor [18], the entire interaction diagram of the cross section can be constructed at given bending moments.

2.3.3 Moment capacity contour for given axial force N and bending moment M_x

In this case, injecting the linear constraints (23) in the nonlinear system (21), parametrizing the bending moment about x-axis through the load factor λ, keeping the axial force constant $N=N_0$ and arranging the system in accordance with the decoupled unknowns, we obtain:

$$\begin{cases} \int_{A_{cs}} \sigma\left(\varepsilon\left(\phi_x,\phi_y\right)\right) dA_{cs} + \sum_{i=1}^{N_{rs}} \sigma\left(\varepsilon_i\left(\phi_x,\phi_y\right)\right) A_{rsi} + \sum_{j=1}^{N_{ps}} \sigma\left(\varepsilon_j\left(\phi_x,\phi_y\right)\right) A_{psj} - N_0 = 0 \\ \int_{A_{cs}} \sigma\left(\varepsilon\left(\phi_x,\phi_y\right)\right) y dA_{cs} + \sum_{i=1}^{N_{rs}} \sigma\left(\varepsilon_i\left(\phi_x,\phi_y\right)\right) y_i A_{rsi} + \sum_{j=1}^{N_{ps}} \sigma\left(\varepsilon_j\left(\phi_x,\phi_y\right)\right) A_{psj} y_j - \lambda M_x = 0 \end{cases} \tag{34}$$

$$M_y = \int_{A_{cs}} \sigma\left(\varepsilon\left(\phi_x,\phi_y\right)\right) x dA_{cs} + \sum_{i=1}^{N_{rs}} \sigma\left(\varepsilon_i\left(\phi_x,\phi_y\right)\right) x_i A_{rsi} + \sum_{j=1}^{N_{ps}} \sigma\left(\varepsilon_j\left(\phi_x,\phi_y\right)\right) A_{psj} x_j \tag{35}$$

Following a similar arc-length strategy as described in the case of interaction diagrams above, the complete moment capacity contour can be obtained under constant axial force. It is important to note that, in this case, maintaining the axial force N constant and scaling just the bending moment, we are in the situation of the non-proportionally applied loading, which involves two loading vectors, one that will be scaled and one fixed. The external loading can be represented in this case by:

$$\mathbf{f}^{ext} = \begin{bmatrix} N_0 \\ 0 \end{bmatrix} + \lambda \begin{bmatrix} 0 \\ M_{x0} \end{bmatrix} = \mathbf{f}_{fixed}^{ext} + \lambda \mathbf{f}_{scaled}^{ext} \tag{36}$$

so that the out of balance force vector becomes:

$$\mathbf{F}(\lambda,\mathbf{\Phi}) = \mathbf{f}^{\text{int}} - \mathbf{f}_{fixed}^{ext} - \lambda \mathbf{f}_{scaled}^{ext} \tag{37}$$

and the basic structure of the arc-length iterative procedure can be maintained [18]. The iteration procedure is conducted with the tangent stiffness matrix computed as:

$$\mathbf{K}_T = \left(\frac{\partial \mathbf{F}}{\partial \mathbf{\Phi}}\right) = \begin{bmatrix} \dfrac{\partial f_1}{\partial \phi_x} & \dfrac{\partial f_1}{\partial \phi_y} \\ \dfrac{\partial f_2}{\partial \phi_x} & \dfrac{\partial f_2}{\partial \phi_x} \end{bmatrix} = \begin{bmatrix} k_{11} & k_{12} \\ k_{21} & k_{22} \end{bmatrix} \tag{38}$$

$$\begin{aligned}
k_{11} &= \frac{\partial f_1}{\partial \phi_x} = \int_{A_{cs}} E_T (y - y_c) dA_{cs} + \sum_{i=1}^{N_{rs}} E_{ti}(y_i - y_c) A_{rsi} + \sum_{j=1}^{N_{ps}} E_{tj}(y_j - y_c) A_{psi} \\
k_{12} &= \frac{\partial f_1}{\partial \phi_y} = \int_{A_{cs}} E_T (x - x_c) dA_{cs} + \sum_{i=1}^{N_{rs}} E_{ti}(x_i - x_c) A_{rsi} + \sum_{j=1}^{N_{ps}} E_{tj}(x_j - x_c) A_{psi} \\
k_{21} &= \frac{\partial f_2}{\partial \phi_x} = \int_{A_{cs}} E_T y (y - y_c) dA_{cs} + \sum_{i=1}^{N_{rs}} E_{ti} y_i (y_i - y_c) A_{rsi} + \sum_{j=1}^{N_{ps}} E_{tj} y_j (y_j - y_c) A_{psi} \\
k_{22} &= \frac{\partial f_2}{\partial \phi_y} = \int_{A_{cs}} E_T y (x - x_c) dA_{cs} + \sum_{i=1}^{N_{rs}} E_{ti} y_i (x_i - x_c) A_{rsi} + \sum_{j=1}^{N_{ps}} E_{tj} y_j (x_j - y_c) A_{psi}
\end{aligned} \tag{39}$$

2.4 Evaluation of tangent stiffness and stress resultant

Based on Green's theorem, the integration of the stress resultant and stiffness coefficients over the cross-section will be transformed into line integrals along the perimeter of the cross-section. For this purpose, it is necessary to transform the variables first, so that the stress field is uniform in a particular direction, given by the current position of the neutral axis [22]. This is achieved by rotating the reference axes x, y to ξ, η oriented parallel to and perpendicular to the neutral axis, respectively (Figure 1) such that:

$$\begin{cases} x = \xi \cos\theta + \eta \sin\theta \\ y = -\xi \sin\theta + \eta \cos\theta \end{cases} \tag{40}$$

where $\tan\theta = \phi_y / \phi_x$. Based on this transformation, the internal forces carried by the compressive concrete and structural steel areas (A_{cs}) can be obtained by the following expressions:

$$
\begin{aligned}
N_{\text{int}} &= \iint_{A_{cs}} \sigma(x,y)dxdy = \iint_{A_{cs}} \sigma(\eta)d\xi d\eta \\
M_{x,\text{int}} &= \iint_{A_{cs}} \sigma(x,y)ydxdy = \iint_{A_{cs}} \sigma(\eta)(-\xi\sin\theta + \eta\cos\theta)d\xi d\eta = M_{\xi,\text{int}}\cos\theta - M_{\eta,\text{int}}\sin\theta \\
M_{y,\text{int}} &= \iint_{A_{cs}} \sigma(x,y)xdxdy = \iint_{A_{cs}} \sigma(\eta)(\xi\cos\theta + \eta\sin\theta)d\xi d\eta = M_{\xi,\text{int}}\sin\theta - M_{\eta,\text{int}}\cos\theta
\end{aligned}
\tag{41}
$$

where N_{int}, $M_{\xi,int}$ and $M_{\eta,int}$ are the internal axial force and bending moments about the ξ and η axis respectively and can be obtained by the following expressions:

$$
\begin{aligned}
M_{\xi,\text{int}} &= \iint_{A_{cs}} \sigma(\eta)\eta d\xi d\eta = \oint_L \sigma(\eta)\xi\eta d\eta \\
M_{\eta,\text{int}} &= \iint_{A_{cs}} \sigma(\eta)\xi d\xi d\eta = \frac{1}{2}\oint_L \sigma(\eta)\xi^2 d\eta \\
N_{\text{int}} &= \iint_{A_{cs}} \sigma(\eta)d\xi d\eta = \oint_L \sigma(\eta)\xi d\xi d\eta
\end{aligned}
\tag{42}
$$

The tangent stiffness matrix coefficients are computed in the same way [18]. As the integration area contour is approximated by a polygon, the integral over the perimeter L, can be obtained by decomposing this integral side by side along the perimeter:

$$
\oint_L h(\eta)\xi^p d\eta = \sum_{i=1}^{nL} \int_{\eta_i}^{\eta_{i+1}} h(\eta)\xi^p d\eta \tag{43}
$$

where nL is the number of sides that forms the integration area. The sides are defined by the ξη co-ordinates of the end-points as shown in Figure 1. When the integration area is a circle with radius R, the integral over the perimeter L can be obtained by decomposing this integral as:

$$
\oint_L h(\eta)\xi^p d\eta = \int_{-R}^{R} h(\eta)\left(R^2 - \eta^2\right)^{p/2} d\eta + (-1)^p \int_{R}^{-R} h(\eta)\left(R^2 - \eta^2\right)^{p/2} d\eta \tag{44}
$$

This leads to a significant saving in imputing the data to describe the circular shapes, without the need to decompose the circular shapes as a series of straight lines and approximate the correct solution when circular boundaries are involved. In order to perform the integral on a determined side of the contour (L_i), polygonal or circular, of the integration area, an adaptive interpolatory Gauss-Lobatto method is used [18].

The conventional steel reinforcement and prestressed tendons are assumed to be discrete points with effective area, co-ordinates and stresses. To avoid double counting of the concrete area that is displaced by the steel bars, the concrete stress at the centroid of the steel bars is subtracted from the reinforcement bar force. In order to identify the various regions in a complex cross-section with different material properties each region with assigned material properties is treated separately [16]. In this way, any composite cross-section with different material properties can be integrated without difficulties.

3. COMPUTATIONAL EXAMPLES

Based on the analysis algorithm just described, a computer program **ASEP** has been developed to study the biaxial strength behaviour of arbitrary prestressed reinforced concrete-steel cross sections. It combines the analysis routine with a graphic routine to display the final results. The computational engine was written using Compaq Visual Fortran. The graphical interface was created using Microsoft Visual Basic 6. Dynamic Link Libraries (DLL) are used to communicate between interface and engine. The many options included make it a user friendly computer program. The graphical interface allows for easy generation of cross-sectional shapes and reinforcement bars, graphical representation of the data, and plotting of the complete stress field over the cross-section, instantaneous position of neutral axis, interaction and moment capacity contour diagrams, etc.

The accuracy and computational advantages of the numerical procedure developed here has been evaluated using several selected benchmark problems analysed previously by other researchers using different numerical methods.

3.1. Example 1: Composite steel-concrete cross-section with arbitrary shape

The composite steel-concrete cross-section depicted in Fig. 8, consists of the concrete matrix, fifteen reinforcement bars of diameter 18 mm, a structural steel element and a circular opening. Characteristic strengths for concrete, structural steel and reinforcement bars are f''_c=30Mpa, f_{st}=355Mpa and f_s=460Mpa, respectively. These characteristic strengths are reduced by dividing them with the corresponding safety factors γ_c=1.50, γ_{st}=1.10 and γ_s=1.15. The stress-strain curve for concrete which consists of a parabolic and linear-horizontal- part was used in the calculation, with the crushing strain ε_0=0.002 and ultimate strain ε_{cu}=0.0035. The Young modulus for all steel sections was 200 GPa while the maximum strain was ε_u=±1%. A bi-linear elasto-perfect plastic stress-strain relationship for the reinforcement bars and structural steel, both in tension and in compression, is assumed. The strain softening effect for the concrete in compression is taken into account, in the present approach, through the parameter γ. This is an example proposed and analysed by Chen et al. [9] and later studied by Charalmpakis and Koumousis [16], Rosati *et.al* [13] and others. The moment-capacity contours (M_x-M_y interaction curve) have been determined under a given axial load N=4120 kN using the approach described in this paper and compared with the results reported in [9], Fig. 9. As it can be seen the results are in close agreement when the bending moments are computed about the plastic centroidal axes of the cross-section. However, the method proposed by Chen [9] does not generate genuinely plane moment-capacity curves, because of convergence problems caused by the fixed axial force. On the contrary, with the proposed approach, the interaction curve can be computed without any convergence difficulties; a maximum of three iterations are necessary to establish the equilibrium, even when the geometric centroid has been chosen as origin of the reference axes or the strain-softening of the concrete in compression is taken into account (γ=0.15). The moment-capacity curves for

these situations are also depicted in the Fig. 9. For these cases, the reference [9] does not present comparative results.

In order to verify the stability of the proposed method a series of analyses have been conducted to determine the interaction curves for different values of bending moment's ratio M_y/M_x =tan(α). The bending moments are computed about the geometric centroidal axes of the cross-section and the strain-softening of the concrete in compression has been modeled (γ=0.15). Figures 10 and 11 shows the interaction diagrams for $\alpha=0^0$, 30^0, 60^0, 90^0. No convergence problems have been encountered using the proposed approach; a maximum of three iterations have been required to complete the entire interaction diagram in each case.

Furthermore, the effects of confinement in the concrete were investigated for different values of degree of confinement. As it can be seen in Figure 12 by reducing the confinement in the concrete the interaction curves indicate lower capacities and the non-convexity of the diagrams is more pronounced. The bending moments are computed about the geometric centroidal axes for a compressive axial force N=10000 kN. This numerical test illustrates the efficiency of the proposed approach and convergence stability.

Let us consider this cross-section subjected to biaxial bending to carry the following design loads: N=4120 kN, M_x=210.5 kN and M_y=863.5 kNm. The distribution of the steel reinforcing bars are shown in Fig. 8, and we consider that all rebars have the same diameter. The procedure described at section 2.2 is used to find the required total steel reinforcement for the cross-section to achieve an adequate resistance for the design loads. As shown in Table 1 the iterative process of design was started with ϕ_x =0 and ϕ_y=0, and A_{tot}=0.005A_g=215 cm^2. The equilibrium tolerance has been taken as 1E-4. After only five iterations, the total area required of the rebars was found to be A_{tot}=34.347 cm^2.

Consequently, the required diameter of the selected rebar is $\Phi_{req} = 2\sqrt{\frac{A_{tot}}{N_b \pi}} = 1.71cm$ which compare very well with the required bar diameter reported by Chen *et.al.* [9], Φ_{req}=1.78cm. Reinforcement bars of diameter 18 mm are thus suitable for this cross-section. In the above computational example, the axial force and bending moments are represented about the plastic centroidal axes of the cross-section. When the design loads are represented about the geometric centroid the total area required of the rebars was found to be A_{tot}=15.674 cm^2. This result has been obtained after only six iterations. For this case the reference [9] does not present comparative results.

3.2. Example 2: Reinforced concrete box cross-section

The box cross-section, depicted in Figure 13.a, consists of the concrete matrix and sixteen reinforcement bars, all rebars having the same diameter. This section is subjected to the following design loads: N=2541.7 kN, M_x=645.6 kNm, and M_y=322.8 kNm. Characteristic strengths for concrete and reinforcement bars are: $f_c^{''} = 23.443\text{MPa}$, f_y=413.69 MPa respectively.

The stress-strain curve for concrete which consists of a parabolic and linear-descending- part was used in the calculation, with the crushing strain ε_0=0.002 and ultimate strain ε_{cu}=0.0038. The Young modulus for reinforcing bars was 200GPa while the maximum strain was ε_u=±1%. A bi-linear elasto-perfect plastic stress-strain relationship for the reinforcement bars, both in tension and in compression, is assumed. The strain softening effect for the concrete in compression is taken into account, in the present approach, through the parameter γ. This problem was also solved by Rodrigues & Ochoa [7]. The procedure described at section 2.2 is used to find the required total steel reinforcement for the cross-

section to achieve an adequate resistance for the above mentioned design loads. The strain softening parameter γ=0.15 for the concrete in compression has been considered in analysis. As shown in Table 2 the iterative process of design was started with ϕ_x =0 and ϕ_y=0, and A_{tot}=0.005A_g=12.25 cm^2. The equilibrium tolerance has been taken as 1E-4. After only six iterations, the total area required of the rebars was found to be A_{tot}=40.586 cm^2. This means that the area required of the selected rebar is 2.536 cm^2 which compare very well with the required area, 2.535 cm^2, reported by Rodrigues & Ochoa [7]. Figure 13.b shows the plastic status of the cross-section associated to the equilibrium between external design loads and internal forces with the total reinforcing area obtained after six iterations. If the effect of tension stiffening is taken into account, considering resistance of tensioned concrete with E_t=33000 MPa, tensile strength f_{cr}=0.234 MPa, concrete cracking strain ε_{cr}=0.000071 and α_1=1, α_2=0.75, the total area required was found, in only five iterations, to be A_{tot}=37.875 cm^2 which is with 7% smaller than the case in which tension stiffening effect was ignored. For this case the reference [9] does not present comparative results.

Figure 14 shows the corresponding interaction curves for both M_x and M_y of this section for α=26.56° (M_y/M_x =tan(α)) with and without tension stiffening effect. Figure 15 shows the moment capacity diagrams for N=2541.7 kN considering different levels of confinement. Rebars of diameter 3/4”≅1.90 cm has been considered in these analyses. As it can be seen, by reducing the confinement in the concrete (γ=*0.15, 0.50*) the interaction curves indicate lower capacities (Fig. 15) and the non-convexity of the diagrams is more pronounced, and also, near the compressive axial load capacity multiple solutions exist in the N-M space when the strain softening is modelled, γ=*0.15* (Fig. 14).

The effects of confinement and creep in the concrete over the total steel reinforcing area are presented in Tables 3 and 4. The section is subjected to the same design loads as in the previously computation. As it can be seen in Table 3 by reducing the confinement in the

concrete (i.e. by increasing the value of γ in descending branch of compressed concrete stress-strain curve) the total reinforcing area increases. No convergence problems have been experienced by the proposed approach, a maximum of seven iterations have been required to determine the reinforcement area for the case when γ=0.5. The effect of creep of the concrete has been investigated by varying the value of crushing strain ε_{c0}. The ultimate strain in the compressed concrete is considered as: $\varepsilon_{cu} = 1.90\varepsilon_{c0}$. As shown in Table 4 the total reinforcement steel area decreases in amount as the concrete creep increases. No convergence problems have been experienced, in all situations, the iterative procedure has converged in only six iterations.

3.3. Example 3: Prestressed box section with circular opening

The prestressed box cross-section, depicted in Figure 16, consists of the concrete core matrix, eight conventional reinforcement bars (R1-R8) each with 25 mm diameter, a circular opening with 60 cm diameter and two perestressed steel tendons each with 50 mm diameter. This is an example proposed and analysed by Kawakami et al. [23] and later studied by Rodrigues and Ochoa [24] and Marmo *et.al* [14].

The EC2 stress-strain curve for compressive concrete was used in the analysis with the crushing strain ε_{c0}=0.00224, ultimate strain ε_{cu}=0.003, compressive strength $f_c^{''} = 40$MPa and modulus of elasticity E_c=33000MPa. Tension stiffening effect, for concrete in tensions, is included in the analysis considering the following characteristics: E_t=26400 MPa, tensile strength f_{cr}=0.344 MPa, concrete cracking strain ε_{cr}=0.00013 and α_1=1, α_2=0.75. A bi-linear elasto-perfect plastic stress-strain relationship for the conventional reinforcement bars, both in tension and in compression, is assumed. The prestressed steel consists on two low-relaxation strands with E_{ps}= 200 GPa, maximum strain ε_u=±1% and ultimate yield stress of f_{pu}=1650 MPa. A bi-linear elasto-perfect plastic stress-strain relationship for the prestressed steel is

assumed with the yield strength of f_y=350 MPa, the Young modulus of 210 GPa while the maximum strain is ε_u=±1%. Initial strain imposed to the presetressed steel during its tensioning $\Delta\varepsilon_p$=0.00381. Figure 17 shows the corresponding interaction curves for both M_x and M_y of this section for α=30° (M_y/M_x =tan(α)) with and without tension stiffening effect. The bending moments are computed about the geometric centroidal axes of the cross-section. As it can be seen, the results obtained in the current paper and those reported in [14] agree closely. No convergence problems have been experienced by the proposed approach, even when the geometric centroid has been chosen as reference axes or the tension stiffening effect has been taken into account, a maximum of three iterations have been required to complete the entire interaction diagram.

Figure 18 presents the moment capacity contours, obtained by the proposed algorithm, for different magnitudes of compressive axial load. As it can be seen, by increasing the value of compressive axial force the interaction curves indicate lower capacities and the non-convexity of the diagrams is more pronounced, as axial load approaches axial load capacity under pure compression. No convergence problems have been encountered, a maximum of five iterations have been required to complete the interaction diagram for the case N=30000 kN.

In order to verify the stability of the proposed method to find the required total steel reinforcement for the cross-section to achieve an adequate resistance for the design loads this example is modified considering additional conventional reinforcement bars (R9-R17) as illustrated in Fig. 16. In this configuration, this section is subjected to biaxial bending and has to be designed to carry out the following design loads: N=10000 kN, M_x=2500 kNm, and M_y=4000 kNm. Table 5 shows the iterative process of design. The equilibrium tolerance has been taken as 1E-4. As it can be seen after only five iterations, the total area required of the rebars was found to be A_{tot}= 94.6442 cm^2. If the effect of tension stiffening is taken into

account, considering resistance of tensioned concrete the total area required was found, in only six iterations, to be A_{tot}=76.955 cm^2 which is with approximately 20% smaller than the case in which tension stiffening effect was ignored. Table 6 shows the effect of initial strain imposed to the presetressed steel over total reinforcement steel area. As it can be seen increasing values of prestressing strain the total area of conventional reinforcement increases. Moreover tension stiffening effect reduces the total reinforcement steel area until 80% in the case of $\Delta\varepsilon_p$=0 and this effect is less pronounced as prestressing strain increase.

3.4. Example 4: Reinforced concrete staircase cross-section

The staircase core section, depicted in Figure 19.a, consists of the concrete matrix and 84 reinforcement bars with the same diameter. This section is subjected to biaxial bending and has to be designed to carry out the following design loads: N=7731.1 kN, M_x=10737.0 kNm, and M_y=11725.5 kNm. Characteristic strengths for concrete and reinforcement bars are: $f_c^{''} = 23.46\text{MPa}$, f_y=220.1 MPa respectively.

The stress-strain curve for concrete which consists of a parabolic and linear-horizontal-part (γ=0) was used in the calculation, with the crushing strain ε_{c0}=0.002 and ultimate strain ε_{cu}=0.003. The Young modulus for reinforcing bars was 290 GPa while the maximum strain was ε_u=±2%. A bi-linear elasto-perfect plastic stress-strain relationship for the reinforcement bars, both in tension and in compression, is assumed. This problem was also solved by Dundar and Sahin [5]. In their analysis the distribution of concrete stress is assumed to be rectangular with a main stress of $f_c^{''} = 23.46\text{MPa}$

As shown in Table 7 the iterative process of design was started with ϕ_x =0 and ϕ_y=0, and A_{tot}=0.005A_g=92.62 cm^2. The equilibrium tolerance has been taken as 1E-4. After only seven iterations, the numerical procedure converges to the solution A_{tot}=316.579 cm^2. This result is in very close agreement with solution A_{tot}=316.257 cm^2 obtained by Dundar and Sahin [5].

Figure 19.b shows the plastic status of the cross-section associated to the equilibrium between external design loads and internal forces with the total reinforcing area obtained after seven iterations. Figure 20 presents the influence of the initial value of A_{tot} over convergence process. As it can be seen, starting the iterative process with A_{tot}=0.01A_g =185.22 cm^2 the numerical procedure converges, in 13 iterations, to the negative solution A_{tot}=-2226.85 cm^2, whereas choosing as initial values A_{tot}=0.005A_g or a very small value, A_{tot}=0.0001, the iterative process converges to the positive and real solution for this case. Figure 21 shows the corresponding moment capacity contour of this section, considering the reinforcement bars with diameter of 2.19 cm, the compressive axial force N=7731.1 kN and different levels of confinement. Nonconvexity of the moment capacity diagrams is revealed even in this case by reducing the confinement in the concrete.

Table 8 presents the variations of the total steel reinforcement area, A_{tot}, and the plastic status of the cross-section, considering different levels of the axial load. The bending moments have the same values as in the previously studied staircase core section (M_x=10737.0 kNm, and M_y=11725.5 kNm). No convergence problems have been encountered using the proposed approach; a low number of iterations have been required to establish the equilibrium, despite the fact that, in all cases, the iterative process has been started with curvatures ϕ_x =0 and ϕ_y =0, and a very restrictive equilibrium tolerance (i.e tol=1E-5), has been considered.

4. CONCLUSIONS

A new computer method has been developed for the rapid design and ultimate strength capacity evaluation of prestressed reinforced and composite steel-concrete cross-sections subjected to axial force and biaxial bending.

Comparing the algorithm developed in this paper, for ultimate strength capacity evaluation, with the existing methods, it can be concluded that the proposed approach is general, can determine both interaction diagrams and moment capacity contours, and, of great importance, it is fast, the diagrams are directly calculated by solving, at a step, just two coupled nonlinear equations and the stability of convergence is not affected by the amount of reinforcement, prestressing and strain softening exhibited by the concrete in compression or tension. Using the proposed method we have found that near the axial load capacity under pure compression, when the strain-softening of the concrete in compression is taken into account, the solution is not unique which implies non-convexity of the failure surface in these situations. Therefore, the proposed approach based on arc-length constraint strategy is essential to assure the convergence of the entire process and to determine all possible solutions.

The iterative algorithm, proposed herein, to design the steel reinforcement of concrete sections subjected to axial forces and biaxial bending, as compared to other iterative methods, is very stable, converging rapidly if the initial value of the required reinforcement area is properly selected. Convergence is assured for any load case, even near the state of pure compression or tension and is not sensitive to the initial/starting values, to how the origin of the reference loading axes is chosen or to the strain softening effect exhibited by the concrete in compression or tension.

The method has been verified by comparing the predicted results with the established results available from the literature. It can be concluded that the proposed numerical method proves to be reliable and accurate for practical applications in the design of composite steel-concrete beam-columns and can be implemented in the advanced analysis techniques of 3D composite frame structures.

Acknowledgement

The writer gratefully acknowledges the support from Romanian National Authority for Scientific Research (ANCS and CNCSIS- Grant PNII-IDEI No. 193/2008) for this study.

5. REFERENCES

[1] Chiorean, C.G., Barsan, G.M., Large deflection distributed plasticity analysis of 3D steel frameworks, *Computers and Structures*, vol. 83, pp. 1555-1571, 2005.

[2] Izzudin, B.A., Lloyd Smith, D., Efficient nonlinear analysis of elasto-plastic 3D R/C frames using adaptive techniques, *Computers and Structures*, vol. 78, pp. 549-573, 2000.

[3] Kwak, K.H., Liauw, T.C., Computerized ultimate strength analysis of reinforced concrete sections subjected to axial compression and biaxial bending, *Computers and Structures*, vol. 21, pp. 1119-1127, 1985.

[4] Rotter, J.M. Rapid exact inelastic biaxial bending analysis, *Journal of Structural Engineering*, ASCE, vol. 111, pp. 2659-267, 1985.

[5] Dundar, C., Sahin, B., Arbitrarily shaped reinforced concrete members subject to biaxial bending and axial load, *Computers and Structures*, vol. 49, pp. 643-662, 1993.

[6] De Vivo, L., Rosati, L., Ultimate strength analysis of reinforced concrete sections subject to axial force and biaxial bending, *Computer Methods in Applied Mechanics and Engineering*, vol. 166, pp. 261-287, 1998.

[7] Rodrigues, J.A. & Aristizabal-Ochoa, J.D. Biaxial interaction diagrams for short RC columns of any cross section, *Journal of Structural Engineering*, ASCE, vol. 125, pp. 672-683, 1999.

[8] Fafitis A., Interaction surfaces of reinforced-concrete sections in biaxial bending, *Journal of Structural Engineering*, ASCE, vol. 127, pp. 840-846, 2001.

[9] Chen S.F., Teng J.G., Chan S.L. Design of biaxially loaded short composite columns of arbitrary section, *Journal of Structural Engineering*, ASCE, vol. 127, pp. 678-685, 2001.

[10] Sfakianakis, M.F., Biaxial bending with axial force of reinforced, composite and repaired concrete cross sections of arbitrary shape by fiber model and computer graphics, *Advances in Engineering Software*, vol. 33, pp. 227-242, 2002.

[11] Bonet, J.L., Romero, M.L., Miguel, P.F., Fernandez M.A., A fast stress integration algorithm for reinforced concrete sections with axial loads and biaxial bending, *Computers and Structures*, vol. 82, pp. 213-225, 2004.

[12] Alfano, G., Marmo, F., Rosati, L., An unconditionally convergent algorithm for the evaluation of the ultimate limit state of RC sections subject to axial force and biaxial bending, *International Journal for numerical methods in Engineering*, vol. 72, pp. 924-963, 2007.

[13] Rosati, L., Marmo, F., Serpieri, R., Enhanced solution strategies for the ultimate strength analysis of composite steel-concrete sections subject to axial force and biaxial bending, *Computer methods in applied mechanics and engineering*, vol. 197, pp. 1033-1055, 2008.

[14] Marmo, F., Serpieri R., Rosati, L., Ultimate strength analysis of prestressed reinforced concrete sections under axial force and biaxial bending, *Computers and Structures*, vol. 89, pp. 91-108, 2011.

[15] Cedolin, L., Cusatis, G., Ecchelli, S., Roveda, M., Capacity of rectangular cross-sections under biaxially eccentric loads, *ACI Structural Journal*, vol. 105, pp. 215-224, 2008.

[16] Charalampakis, A.E., Koumousis, V.K., Ultimate strength analysis of composite sections under biaxial bending and axial load, *Advances in Engineering Software*, vol. 39, pp. 923-936, 2008.

[17] Pallares, L., Miguel, P.F., Prada, M.A.F, A numerical method to design reinforced concrete sections subjected to axial forces and biaxial bending based on ultimate strain limits, *Engineering Structures*, vol. 31, pp. 3065-3071, 2009.

[18] Chiorean, C.G., Computerised interaction diagrams and moment capacity contours for composite steel-concrete cross-sections, *Engineering Structures*, vol. 32, pp. 3734-3757, 2010.

[19] Vecchio, F.J., Collins, M.P., The modified compression field theory for reinforced concrete elements subjected to shear, *ACI Journal*, vol. 83, pp. 219-231, 1986.

[20] Eggert, G.M., Dawson, P.R., and Mathur K.K., An adaptive descent method for nonlinear viscoplasticity. *Int. J. Num. Meth. Engng* vol. 31, pp. 1031–1054, 1991.

[21] Crisfield, M.A. Non linear finite element analysis of solids and structures, Wiley, Chichester, 1991.

[22] Chiorean, C.G., A fast incremental-iterative procedure for inelastic analysis of RC cross-sections of arbitrary shape, *Acta Technica Napocensis: Civil Engineering & Architecture*, vol. 47, pp. 85-98, 2004.

[23] Kawakami, M., Tokuda H., Kagaya M., Hirata M., Limit states of cracking and ultimate strength of arbitrary concrete sections under biaxial loading, ACI Structural Journal, vol. 82, pp. 203-2012, 1985.

[24] Rodrigues J.A., Arisizabal-Ochoa, J.D., Partially and fully prestressed concrete sections under biaxial bending and axial load, ACI Structural Journal, vol. 97, pp. 553-563, 2000.

FIGURES AND TABLES

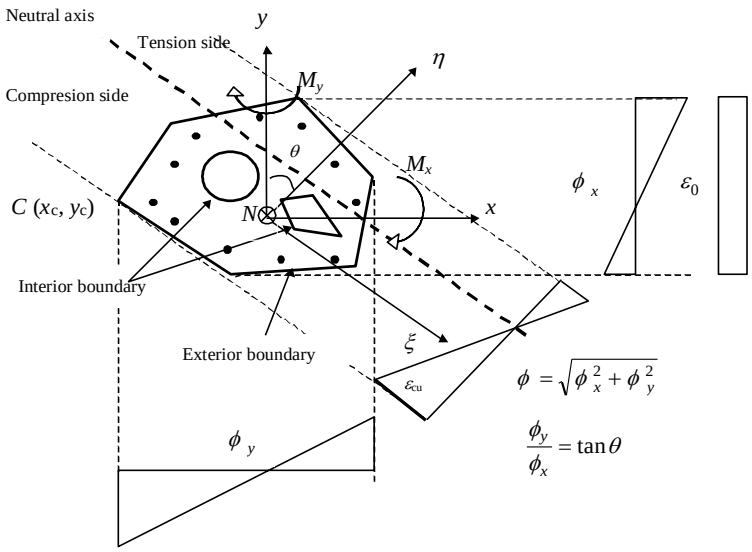

Figure 1. Model of arbitrary composite cross-section.

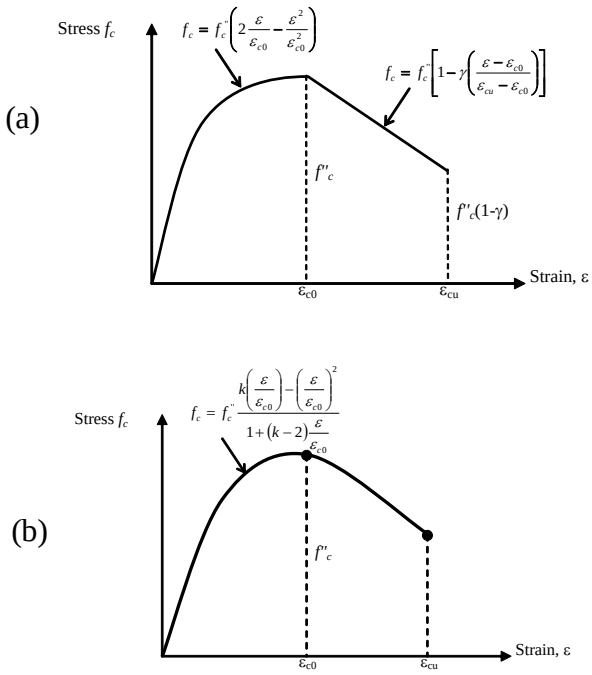

Figure 2. Stress-strain relationships for concrete in compression: (a) combination of second-degree parabola and straight line; (b) EC2 stress-strain law.

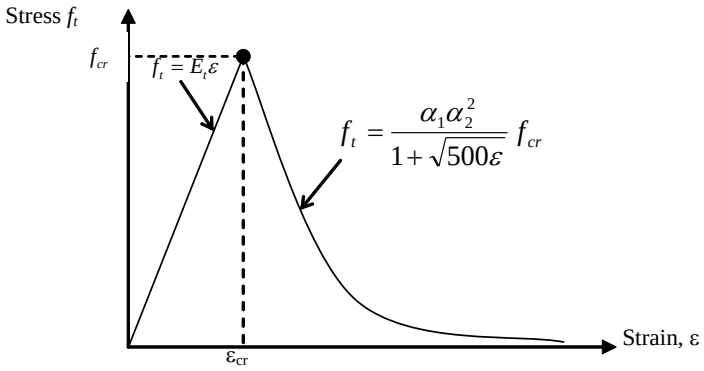

Figure 3. Stress-strain relationships for concrete in tension.

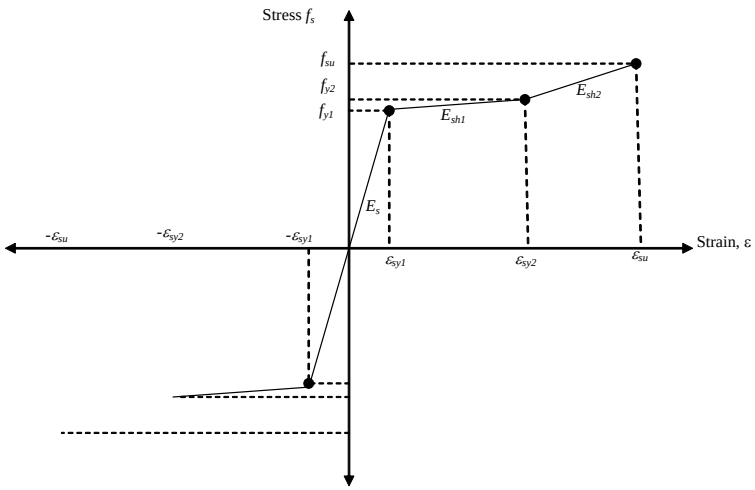

Figure 4. Stress-strain relationships for steel reinforcement.

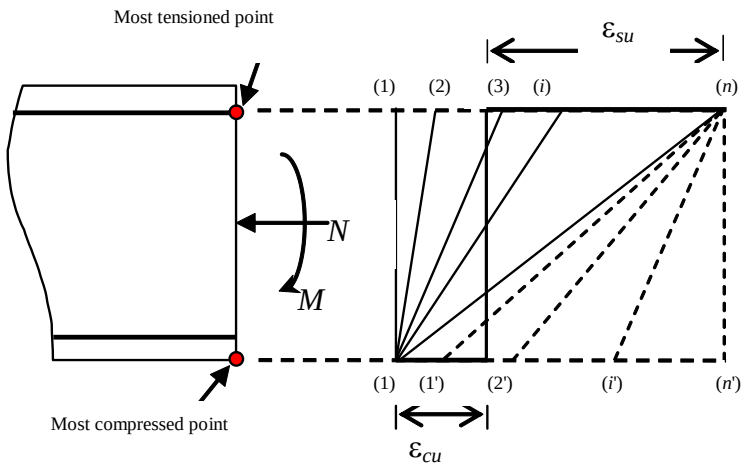

Figure 5. Strains profile at failure.

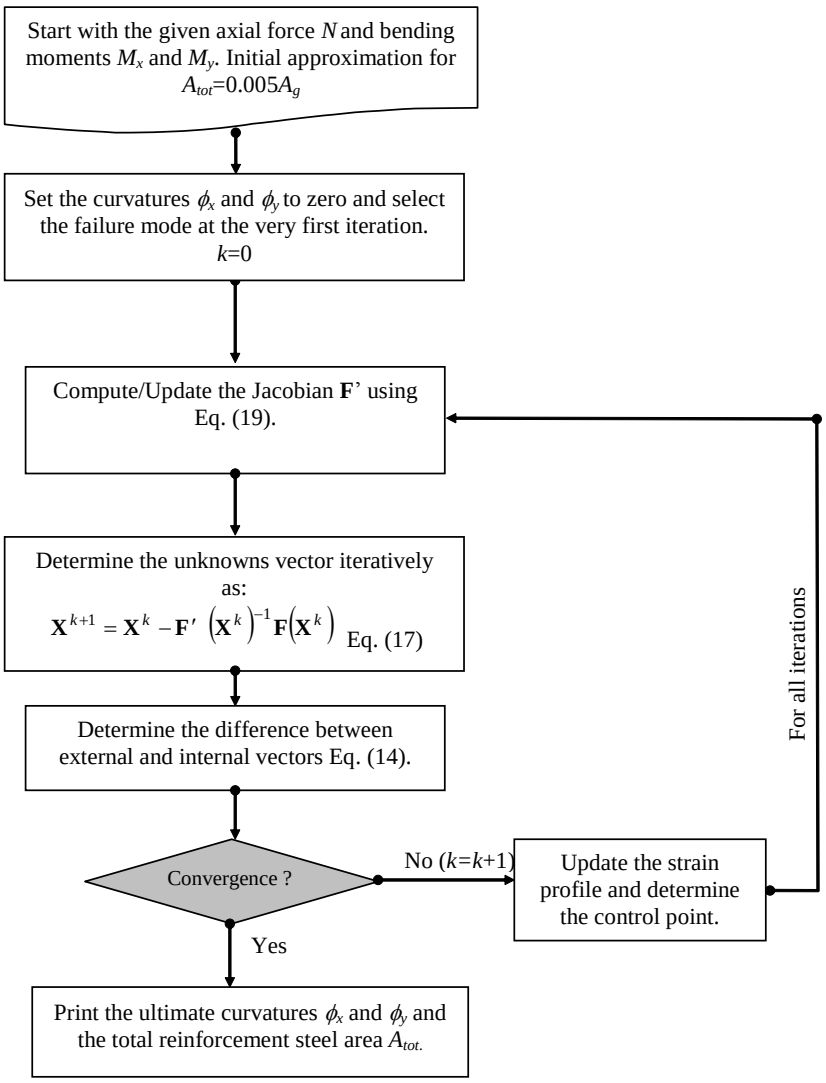

Figure 6. Flowchart for design procedure.

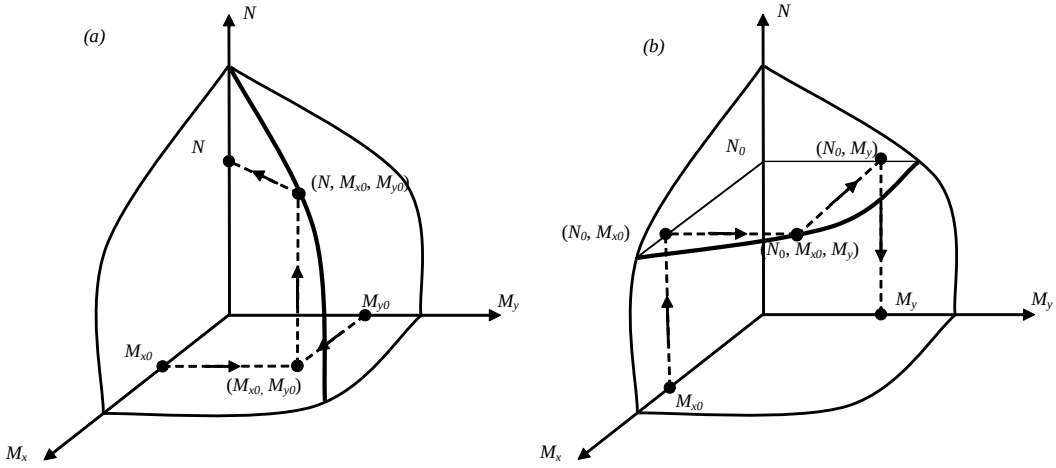

Figure 7: Solution procedures. (a) Interaction diagrams for given bending moments; (b) Moment-capacity contours for given axial force and bending moment M_x.

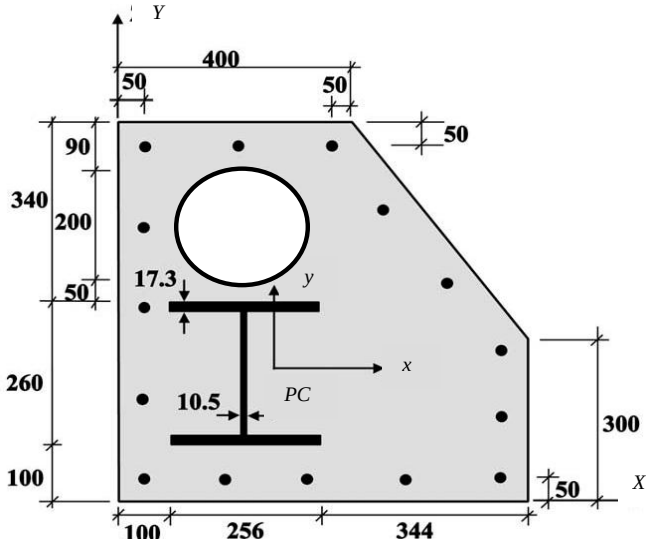

Figure 8. Example 1. Composite steel-concrete cross-section.

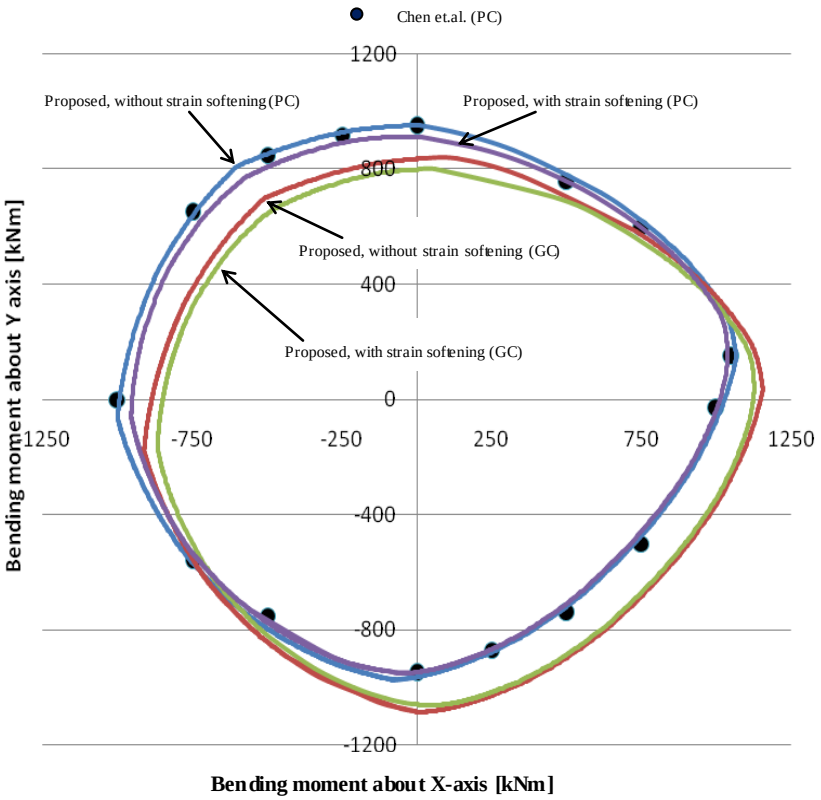

Figure 9. Moment capacity contour with axial load *N*=4120 kN.

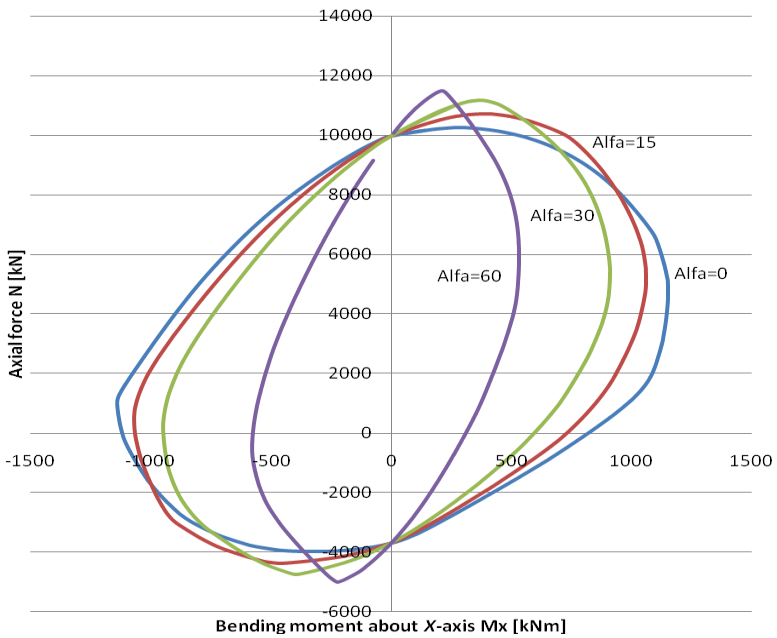

Figure 10. Biaxial interaction diagrams. Bending moments about *X*-axis.

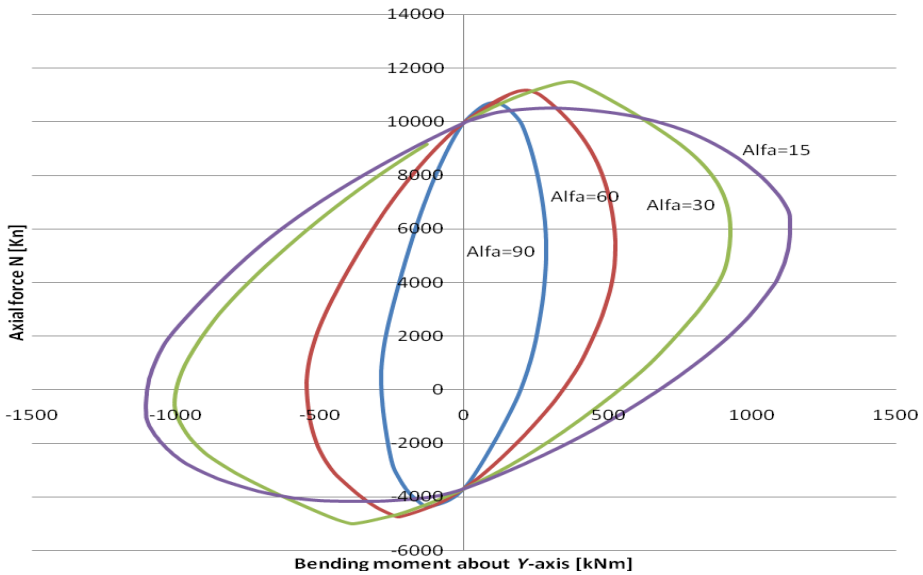

Figure 11. Biaxial interaction diagrams. Bending moments about *Y*-axis.

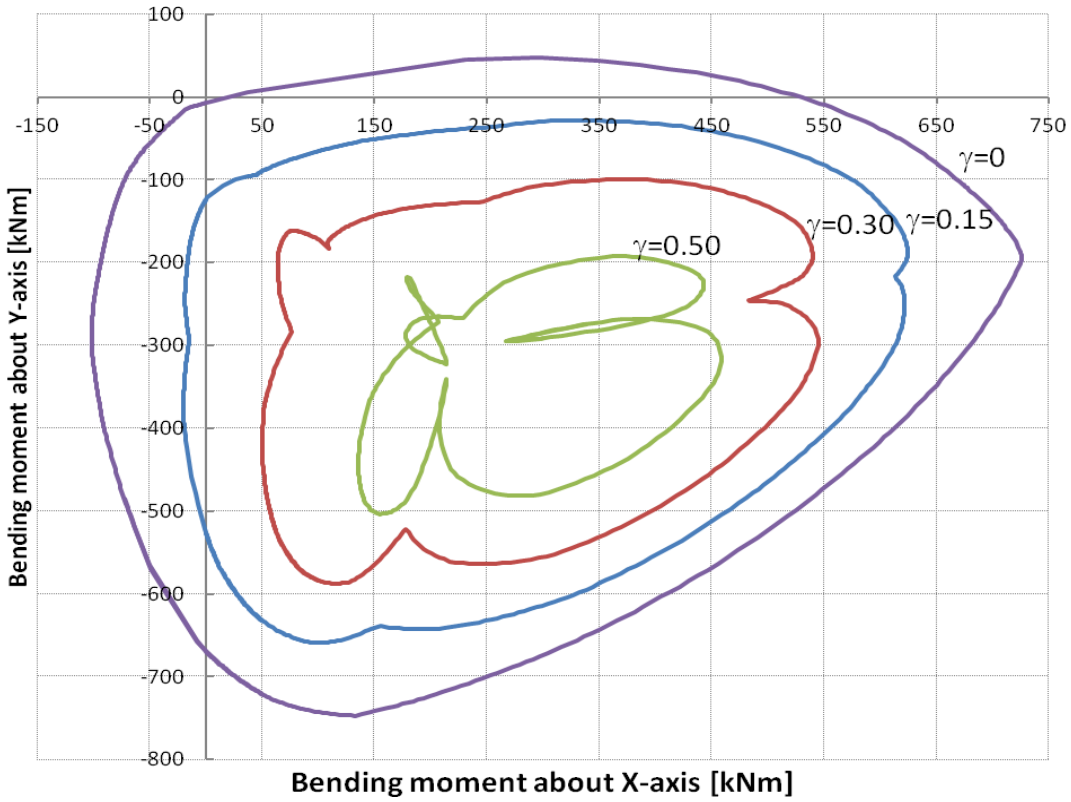

Figure 12. Moment capacity contours with compressive axial load *N*=10000 kN for different values of degree of confinement.

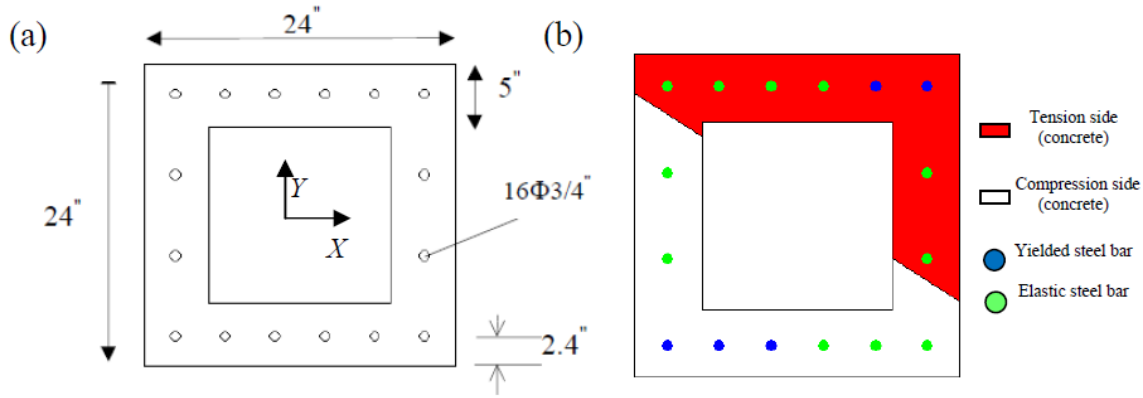

Figure 13. Example 2. (a) Biaxially loaded box cross-section; (b) Plastic status of section under design loads and A_{tot}=40.586 cm^2.

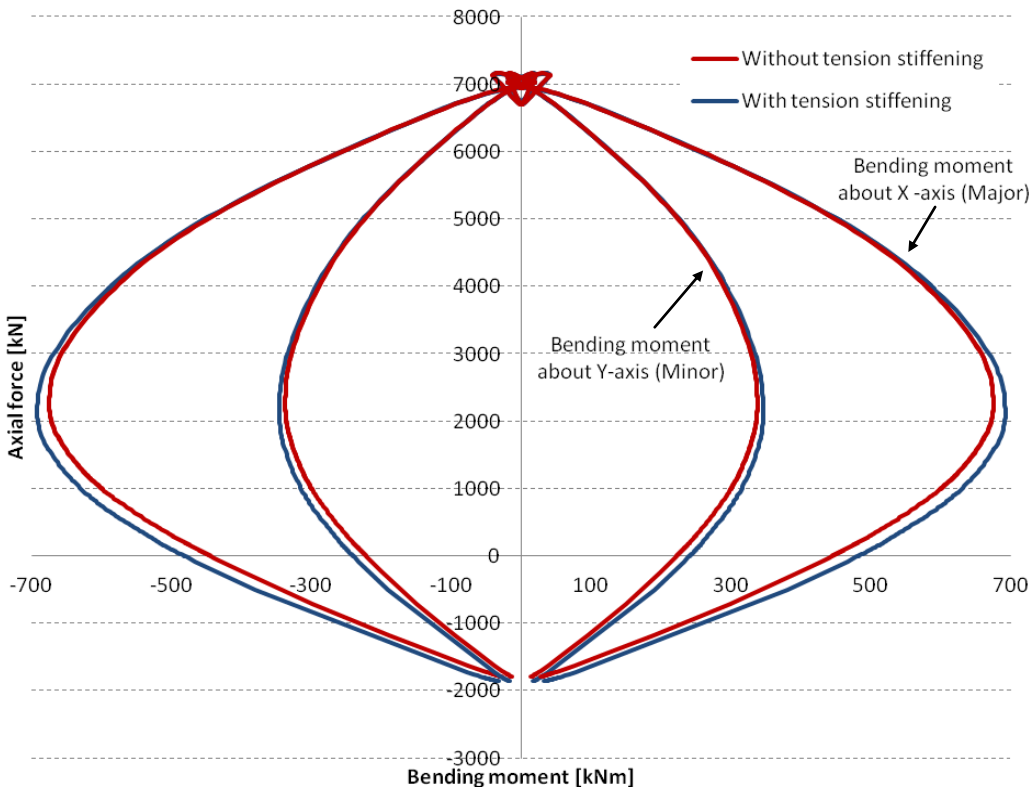

Figure 14. Biaxial interaction curves for box cross-section α=26.56°.

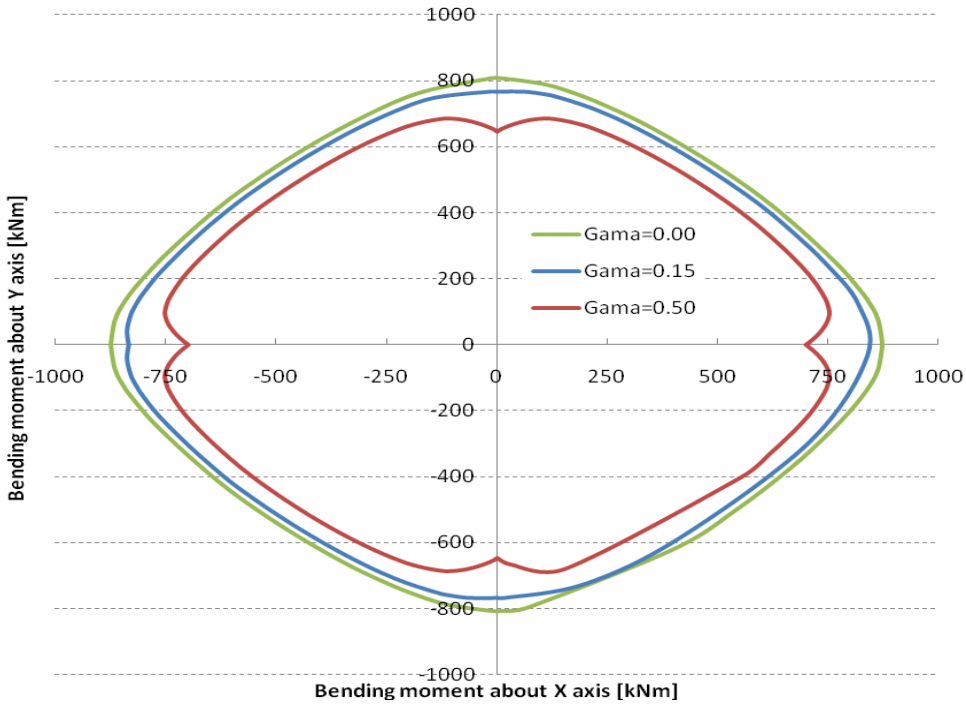

Figure. 15. Moment capacitiy contours of box cross-section with compressive axial force *N*=2541.7 kN.

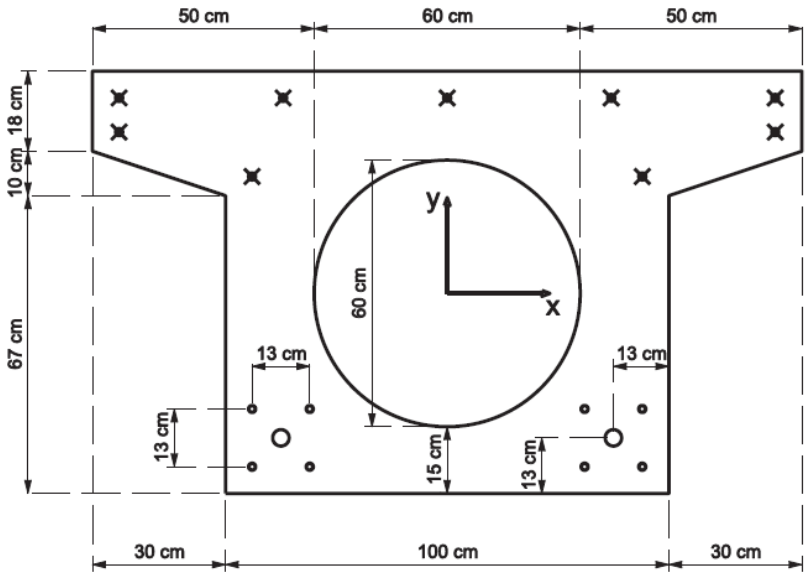

Figure 16. Example 3: Prestressed box section with circular opening

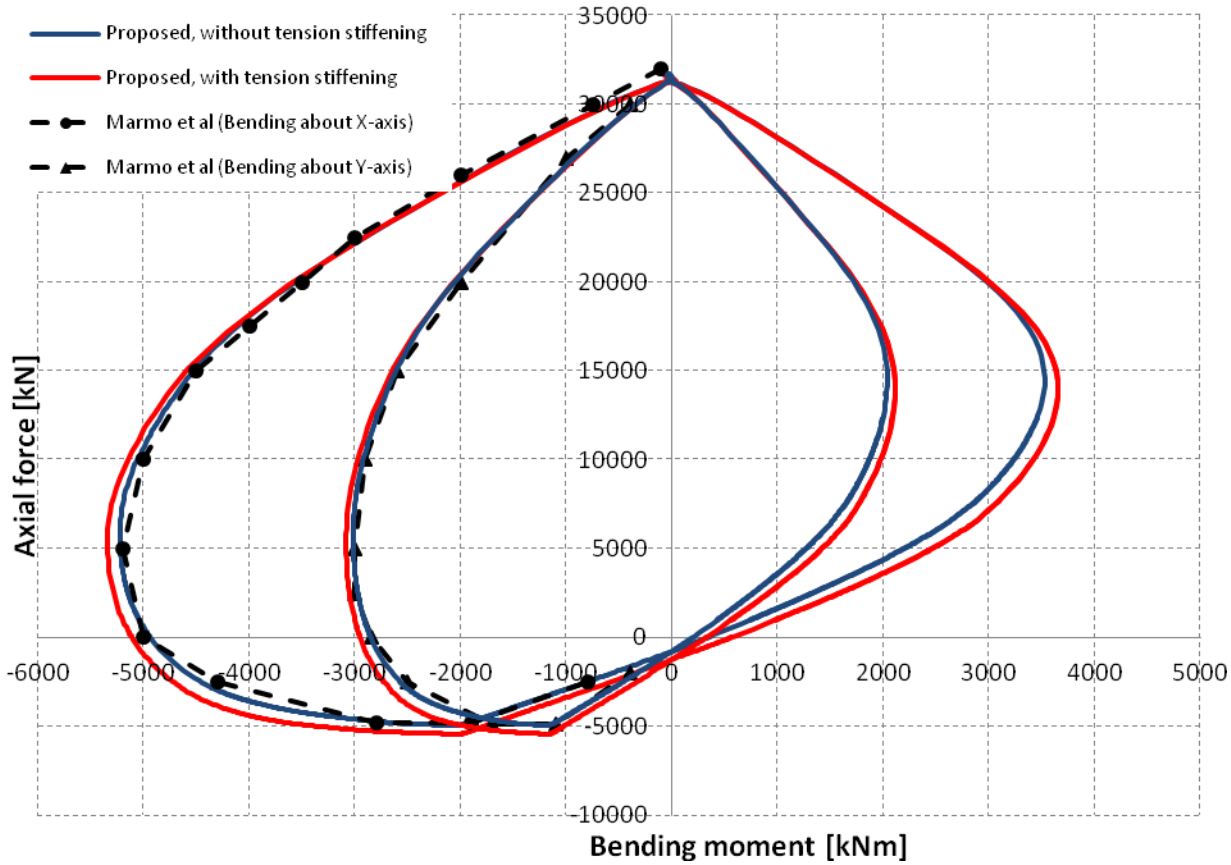

Figure 17. Biaxial interaction diagrams for α=30°.

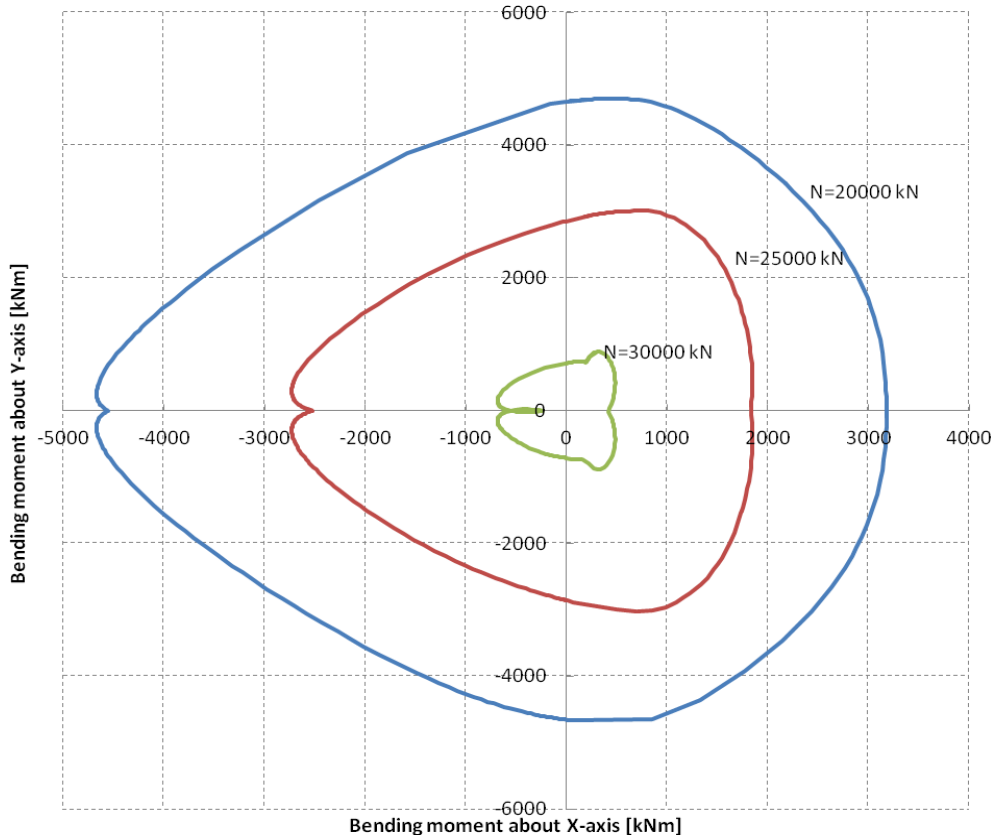

Figure 18. Moment capacities contours for different values of compressive axial load.

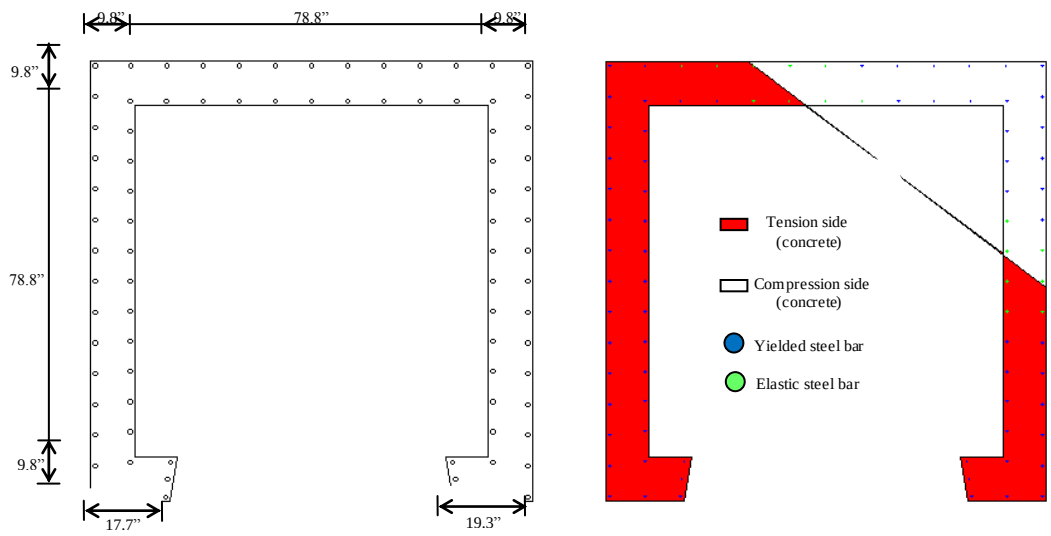

Figure 19. Example 4. (a) Staircase core section; Plastic status of section under design loads and A_{tot}=316.579 cm^2.

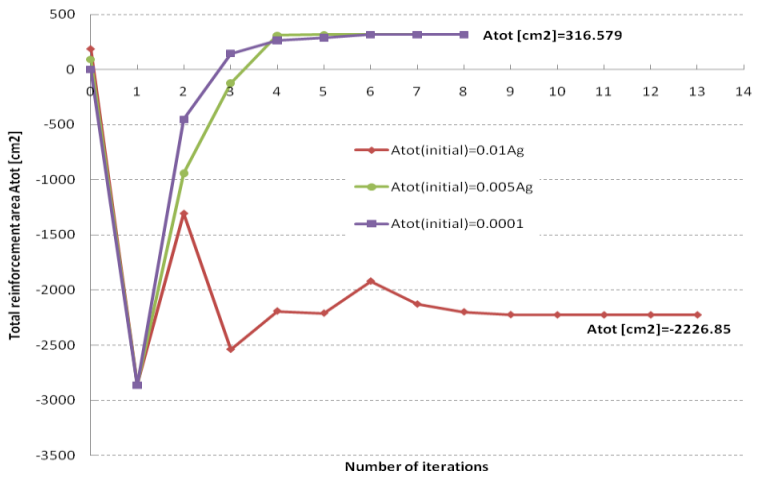

Figure 20. Influence of the initial value of A_{tot} over convergence process.

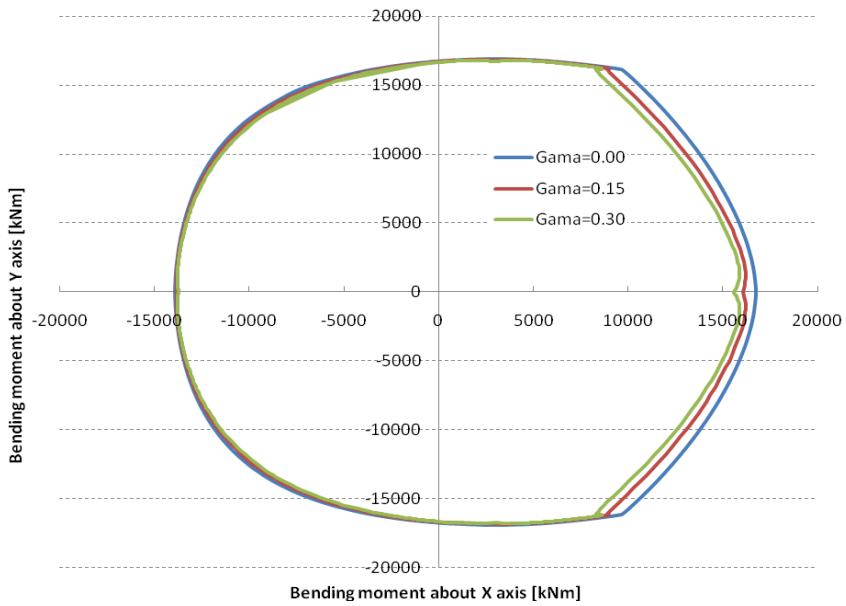

Figure 21. Moment capacity contours for staircase cross-section with compressive axial force

N=7731.1 kN

TABLES

Table 1: Main parameters involved in the design of composite steel-concrete section

Iteration	ϕ_x	ϕ_y	A_{tot} [cm^2]	Error (Eq. 20)
Initial	0.000	0.000	$0.005A_g$=215	1.000
1	2.977E-5	7.197E-5	144.835	1.08254
2	2.9187E-5	7.9279E-5	20.168	0.8347
3	2.9093E-5	8.6250E-5	33.351	0.1060
4	2.9003E-5	8.5837E-5	34.350	0.010026
5	2.9000E-5	8.5850E-5	34.347	0.000082

Table 2. Example 2: Main parameters involved in the iterative process.

Iteration	ϕ_x	ϕ_y	A_{tot} [cm^2]	Error (Eq. 20)
Initial	0.000	0.000	$0.005A_g$=12.25	1.000
1	1.089E-4	5.576E-5	115.41	1.000146
2	6.426E-5	5.264E-5	30.816	0.599621
3	7.102E-5	4.550E-5	39.682	0.173854
4	7.084E-5	4.559E-5	40.556	0.007475
5	7.0834E-5	4.5583E-5	40.585	0.000266
6	7.08345E-5	4.5583E-5	40.586	0.00000856

Table 3. Example 2: Confinement effect over A_{tot}

γ	A_{tot} [cm^2]	No. of iterations
0	37.521	5
0.15	40.586	6
0.30	43.788	7
0.50	48.428	7

Table 4. Example 2: Creep effect over A_{tot}

ε_{c0} (ε_u=1.9ε_{c0})	A_{tot} [cm^2]	No. of iterations
0.002	40.586	6
0.003	36.307	6
0.004	35.189	6
0.005	34.578	6
0.007	34.115	6

Table 5. Example 3: Main parameters involved in the iterative process.

Iteration	ϕ_x	ϕ_y	A_{tot} [cm^2]	Error (Eq. 20)
Initial	0.000	0.000	0.005A_g=44.87	1.000
1	2.8680E-5	2.23386E-5	255.378	1.031139
2	3.0268E-5	2.30956E-5	96.4584	0.483532
3	3.12286E-5	2.38899E-5	94.2212	0.0218453
4	3.12569E-5	2.39271E-5	94.6242	0.0005905368
5	3.12562E-5	2.39269E-5	94.6442	0.000062789

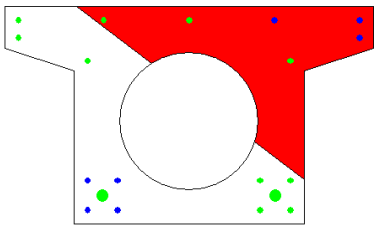

Plastic status of section at equilibrium

Table 6. Effect of prestressing strain over total reinforcement steel area

$\Delta\varepsilon_p$	A_{tot} [cm^2] (whithout tension stiffening)	A_{tot} [cm^2] (whith tension stiffening)
0.000	42.728	23.773
0.001	52.770	33.462
0.002	65.209	46.453
0.003	80.123	62.130
0.004	98.257	80.663
0.005	118.578	102.273
0.006	142.390	126.555

Table 7. Example 4: Main parameters involved in the iterative process.

Iteration	ϕ_x	ϕ_y	A_{tot} [cm^2]	Error (Eq. 20)
Initial	0.000	0.000	$0.005A_c$=92.62	1.000
1	-5.644E-6	-7.830E-6	-2858.381	1.006109
2	-1.376E-5	-6.785E-5	-940.168	0.249642
3	-2.048E-5	-1.466E-5	-124.761	0.331049
4	-2.460E-5	-1.814E-5	310.799	0.183181
5	-2.333E-5	-1.772E-5	315.943	0.0357735
6	-2.335E-5	-1.773E-5	316.572	0.0001169
7	-2.3352E-5	-1.7732E-5	316.579	0.0000232

Table 8. Example 4: Variations of the total steel reinforcement area with different levels of the axial load.

N [kN]	A_{tot} [cm^2]	No. of iterations	Plastic status
1000	559.741	6	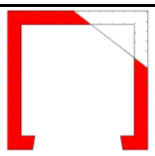
10000	242.105	5	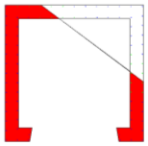
20000	12.814	4	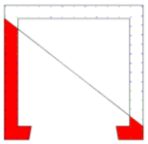
30000	110.903	4	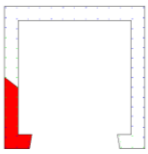
40000	505.181	6	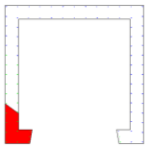
50000	987.723	7	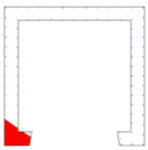
-1000	636.151	6	
-10000	994.658	7	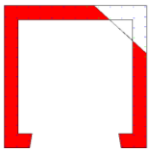

-20000	1409.775	7